

Review

Visible Light Communication System Technology Review: Devices, Architectures, and Applications

Tai-Cheng Yu ^{1,†}, Wei-Ta Huang ^{1,†} , Wei-Bin Lee ^{2,3}, Chi-Wai Chow ¹, Shu-Wei Chang ^{1,4,*}
and Hao-Chung Kuo ^{1,2,*} 

¹ Department of Photonics, College of Electrical and Computer Engineering, National Yang Ming Chiao Tung University, Hsinchu 30010, Taiwan; taicherng@gmail.com (T.-C.Y.); aaronhuang.dop09g@nctu.edu.tw (W.-T.H.); cwchow@faculty.nctu.edu.tw (C.-W.C.)

² Semiconductor Research Center, Hon Hai Research Institute, No. 2, Ziyou St., Tucheng Dist., New Taipei City 23678, Taiwan; wei-bin.lee@foxconn.com

³ Department of Information Engineering and Computer Science, Feng Chia University, Taichung 40724, Taiwan

⁴ Research Center for Applied Sciences, Academia Sinica, Taipei 11529, Taiwan

* Correspondence: swchang@sinica.edu.tw (S.-W.C.); hckuo@faculty.nctu.edu.tw (H.-C.K.)

† The authors contributed equally to this work.

Abstract: Visible light communication (VLC) is an advanced, highly developed optical wireless communication (OWC) technology that can simultaneously provide lighting and high-speed wireless data transmission. A VLC system has several key advantages: ultra-high data rate, secure communication channels, and a lack of interference from electromagnetic (EM) waves, which enable a wide range of applications. Light-emitting diodes (LEDs) have been considered the optimal choice for VLC systems since they can provide excellent illumination performance. However, the quantum confinement Stark effect (QCSE), crystal orientation, carrier lifetime, and recombination factor will influence the modulation bandwidth, and the transmission performance is severely limited. To solve the insufficient modulation bandwidth, micro-LEDs (μ -LEDs) and laser diodes (LDs) are considered as new ideal light sources. Additionally, the development of modulation technology has dramatically increased the transmission capacity of the system. The performance of the VLC system is briefly discussed in this review article, as well as some of its prospective applications in the realms of the industrial Internet of Things (IoT), vehicle communications, and underwater wireless network applications.

Keywords: visible light communication; laser diode; light-emitting diode; modulation scheme; optical receiver; quantum communication



Citation: Yu, T.-C.; Huang, W.-T.; Lee, W.-B.; Chow, C.-W.; Chang, S.-W.; Kuo, H.-C. Visible Light Communication System Technology Review: Devices, Architectures, and Applications. *Crystals* **2021**, *11*, 1098. <https://doi.org/10.3390/cryst11091098>

Academic Editors: Pengfei Tian and Zheng Gong

Received: 20 August 2021

Accepted: 7 September 2021

Published: 9 September 2021

Publisher's Note: MDPI stays neutral with regard to jurisdictional claims in published maps and institutional affiliations.



Copyright: © 2021 by the authors. Licensee MDPI, Basel, Switzerland. This article is an open access article distributed under the terms and conditions of the Creative Commons Attribution (CC BY) license (<https://creativecommons.org/licenses/by/4.0/>).

1. Introduction

Electromagnetic waves have an extensive range of applications, including cell phone communications, wireless radio broadcast, Wi-Fi, etc. Depending on the wavelength, electromagnetic waves can be roughly divided into radio waves, infrared rays, visible light, ultraviolet rays, etc. Though radio frequency (RF) is not susceptible to low interference, it is capable of wide area coverage [1]. Nevertheless, RF has several disadvantages, such as interference, bandwidth limitations, safety issues, transmission power limitations, and a crowded radio spectrum [2–5]. Therefore, visible light communication (380 to 780 nm) has been developed to solve these challenges as an alternative solution to the problem mentioned above. Wireless optical communication technology is characterized by its emphasis on the realization of high-frequency bandwidth communication capacity, which is significantly greater than the current radio wireless communication frequency. In the past ten years, light fidelity (Li-Fi) technology, which combines illumination and communication, has risen to the forefront of study.

Optical Wireless communication (OWC) has two main advantages: one is that it won't be interfered with by electromagnetic waves. Despite the fact that current flight regulations allow passengers to use electronic devices on planes and vital medical equipment in hospitals, and copper nets are embedded in the walls to prevent mobile phone interference, there are still some chances for interference. On the other hand, wireless optical communication in these sensitive places can avoid interference. The other advantage is power saving; it is more power efficient to turn on and off a LED/LD than to use RF wireless radio frequency to transmit signals. Hand-held devices have limited battery power, so it is more advantageous to use optical wireless communication to transmit signals. Li-Fi technology design is directly combined with the LED bulb of the skylight board to enable hotspot for indoor wireless internet access, and most mobile phones have LED flashes and CMOS camera lenses, which means that they can potentially receive and send information. The beam steering and VLC position combination is a promising solution to directionality between the light source and the receiver [6]. Although the active components of the VLC system will inevitably increase the power consumption, alignment difficulties, cost, and volume of the mobile device, these can be mitigated by utilizing a modulated retroreflector (MRR) in the mobile device; this has been successfully demonstrated recently [7]. In the future, mobile phones may be able to easily exchange information; a schematic of a VLC System is shown in Figure 1.

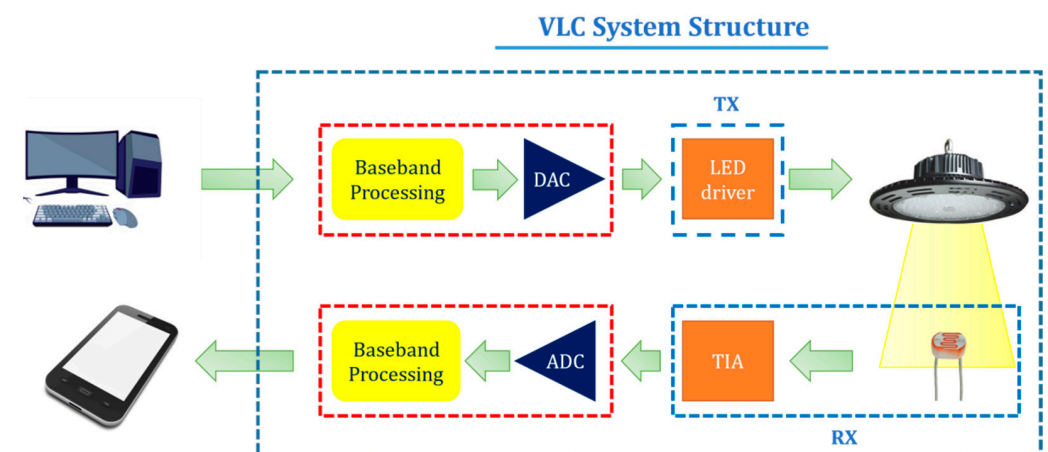


Figure 1. A schematic of a VLC System (Tx: Transmitter; Rx: Receiver; DAC/ADC: Digital/Analog converter; TIA: Transimpedance amplifier).

Visible light communication is mainly composed of two components: an optical transmitter (Tx) and optical receiver (Rx), as shown in Figure 1. After preprocessing and encoding, a binary bit stream drives the light source (LED/LD), and the electrical signals are converted into optical signals through modulation. Signal distortion generated by other channels is compensated by using pre-processing. The equalization technology can increase the response bandwidth of the LED and increase the transmission data rate. The receiver's post-equalization can compensate for other channel losses, such as phase noise. High-order coding modulation techniques were used to increase the transmission rate and spectrum efficiency.

The light sources that are predominantly used in VLC systems are LEDs and laser diodes. White light is preferred for indoor illumination; hence, red, green, and blue LEDs (RGB-LEDs) are mixed to generate white light sources, or yellow phosphors convert blue LED output into white light sources. When compared to RGB three-color hybrid LEDs, employing yellow phosphor Gallium Nitride (GaN) blue LEDs can minimize light source complexity and system cost. However, when the blue photon hits yellow phosphor [8–11], the transition causes a relatively reduced penetration power and frequency modulation bandwidth, thereby limiting the signal-to-noise ratio (SNR) and transmission capacity of Li-Fi systems. In 2020, J. Vučić et al. modulated the limited bandwidth of an LED with Discrete

Multitone (DMT) format, achieving 513 Mbit/s of data rate [12]. In 2012, Khalid et al. reached a data rate of 1 Gbit/s with a phosphorescent white LED by the utilization of a DMT modulation scheme [13]. To improve spectrum utilization, Li-Fi systems mostly use carrier-less amplitude and phase (CAP) and M-ary quadrature-amplitude-modulation (M-QAM) as the modulation format. In 2013, Wu et al. used CAP and QAM-orthogonal frequency-division multiplexing (OFDM) to modulate an RGB-LED, reaching a data rate of 2.93 and 3.22 Gbit/s, respectively [14]. However, the coherence, noise performance, and direct modulation bandwidth of the traditional LEDs were all hampered by the spontaneously radiating photons of the active region stimulated by the photons. To overcome the problems mentioned above, resonant cavity LEDs or micro-LED arrays (μ -LEDs) have been proposed due to their high internal quantum efficiency (IQE), light extraction rate, and variable modulation bandwidth. Since the RC constant of the device cannot limit the bandwidth of the μ -LED [15] and the GaN μ -LED is a much smaller LED ($<100 \mu\text{m}$), it has been proven to provide better white light than traditional LEDs, with a higher output intensity and wider modulation bandwidth [16,17].

Laser diodes (LDs) are another light source often employed in VLC systems. They have stronger coherence, narrower spectral linewidth, and larger modulation bandwidth, making them more suited for data rates exceeding Gbit/s [18,19]. Unlike LEDs, which can only provide up to a few hundred MHz of usable bandwidth, a commercial transistor-outline can (TO-can)-packaged GaN blue LD was reported in 2013 carrying 2.5 Gbit/s of error-free on-off keying (OOK) transmission, which can provide a VLC system with 1.4 GHz of bandwidth [20]. In 2013, Chen et al. demonstrated a bidirectional VLC that can provide 2.5 Gbit/s 16-QAM OFDM, using a red laser pointer [21]. To increase the data rate, in 2013, Chi et al. achieved 9 Gbit/s VLC in a 5 m point-to-point (PtP) free space link by utilizing 64-QAM OFDM to modulate a GaN blue LD [22]. The lighting function of an LD is similar to an LED, which is realized by covering the output end of blue LD with yellow phosphor or using the collimated beam of mixed R/G/B LD. In 2015, Lee et al. demonstrated a non-return-to-zero OOK (NRZ-OOK) data stream that transmitted at a data rate of 2 Gbit/s using a blue LD covered with a yellow phosphor [23]. In the same year, Retamal et al. achieved a data rate of 4 Gbit/s by embedding the yellow fluorescence of the blue LD into remote color conversion [24]. In 2015, Chi et al. also illustrated a blue LD-based white light converted by a phosphorous diffuser, with a correlated color temperature (CCT) of 5217K, which can transmit 16-QAM OFDM data at a data rate of 5.2 Gbit/s in a 0.6 m free space channel [25]. Additionally, Tsonev et al. expected to achieve a data rate exceeding 100 Gbit/s by using an R/G/B hybrid LD light source for white light VLC carrying a QAM-OFDM signal [26]. In 2017, Wu et al. achieved an 8 Gbit/s data rate with 16-QAM OFDM over 0.5 m free space by using a commercial R/G/B TO-can-packaged LD [27]. These illustrations suggested that visible light LDs have greater data transmission potential than LEDs and that this potential will grow in the future. Mainstream white light VLC light sources will be achieved by using laser and color mixing technology, and a brief comparison of light source used in VLC systems is presented in Table 1.

Table 1. Comparison of light source used in the VLC system.

Light Source	Size (mm ²)	Limiting Factor	Bandwidth	Power	Eye Safe
LED	0.1~1	τ_{RC} (~1 ns)	~10 MHz	>1 W	Yes
μ -LED	<0.01	$\tau_{carrier}$ (~1 ns)	<1.5 GHz	~ μ W	Yes
Laser diode	<0.2	τ_{Photon} (~1 ps)	10~20 GHz	>1 W	No
Laser light	~0.01	τ_{Photon} (~1 ps)	10~20 GHz	>1 W	Yes

2. VLC Transmitter Light Source

2.1. Theoretical Background of LED for VLC Application

At present, most of the light sources used in VLC systems are white light LEDs, which are mainly divided into two categories, RGB-LED and phosphor-converted (pc)-LED. RGB-LED is realized by the utilization of three primary color phosphors which are excited

by violet or ultraviolet LEDs; another approach is to package red, green, and blue chips together to emit white light (RGB-LED), as shown in Figure 2a. On the other hand, a pc-LED converts the light source into white light by exciting the yellow phosphor with a blue LED chip, as shown in Figure 2b [28,29].

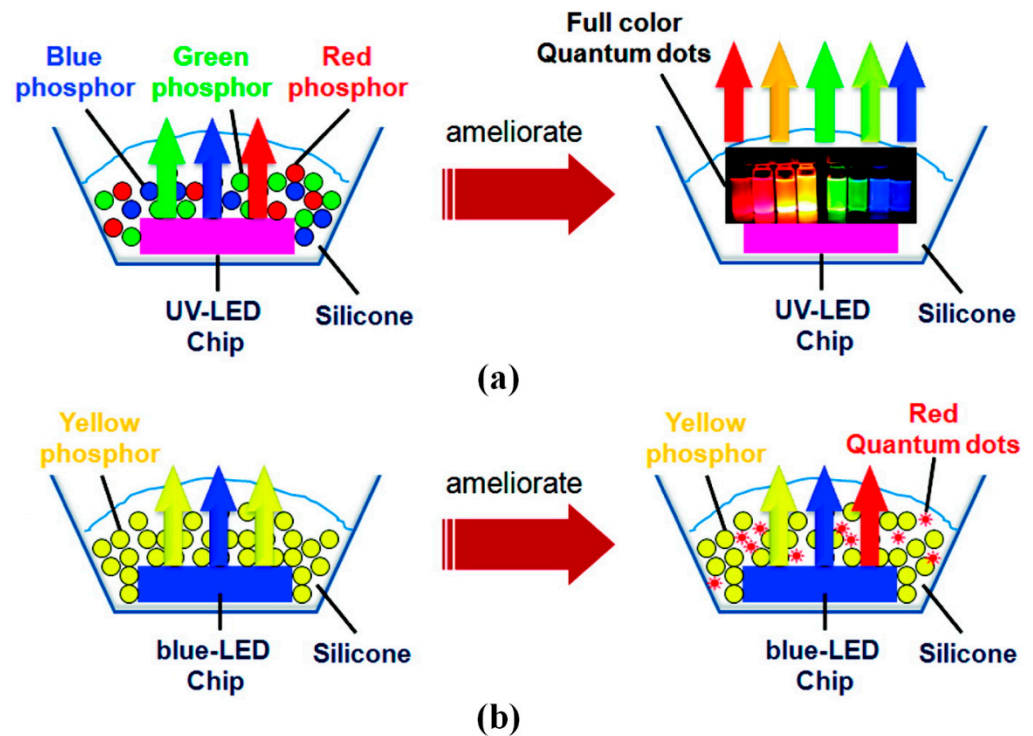


Figure 2. Structures for generating white light from fluorescent materials, based on (a) UV chip and (b) blue chip. Reprinted with permission from [29]. Copyright 2011, American Chemical Society.

Studying the modulation characteristics of the LED device is critical to improving the performance of the new Li-Fi system. The modulation bandwidth of the LED determines the channel capacity and data rate of the communication system. The definition of LED modulation bandwidth is the frequency when the AC optical power output by the LED drops to 50% of a certain reference frequency value (-3 dB). As the photoelectric response of a pc-LED is relatively behindhand [30], the modulation bandwidth of the Li-Fi light source is limited to a few MHz, therefore limiting the data rate of the entire system; even the use of a blue filter failed to improve the defects of the light source.

Use of a higher modulation bandwidth by using wavelength division multiplexing (WDM) with three different wavelengths of light increases the channel capacity of RGB-LEDs. The terminal receives three wavelengths of light through filters of each wavelength, which significantly improves the transmission efficiency. However, different colors of RGB-LED have different operating temperatures, depending on the output light flux. To achieve independent color operating at different temperatures, the feedback loop and each single-color LED's driving current need to be controlled individually, which leads to higher cost and a more complex modulation circuit.

The response rate and modulation bandwidth of the LED are influenced by the carrier lifetime. In addition, increasing the radiation recombination rate of electrons and holes and reducing the spontaneous radiation lifetime of carriers is a conventional approach for designing a modulation circuit and minimizing the RC delay. The spontaneous emission lifetime of carriers has been decreased by increasing the injected carrier concentration, which can be achieved by increasing the injection current and delta doping. Under high injection current, as the injected carrier concentration increases, the exciton recombination probability increases, the radiation recombination carrier lifetime decreases, and the electro-

optical conversion responds quickly. Delta doping technology also results in high carrier injection, thereby reducing carrier lifetime and improving modulation bandwidth at the same current density.

Due to the built-in piezoelectric polarization of the LED, the traditional polar LED grown on the c-plane has limited bandwidth, especially in the green spectral region [31]. The polarization in the c-plane-oriented InGaN quantum well produces a robust quantum confinement Stark effect (QCSE), which separates electrons and holes, thereby increasing the time for radiation recombination [31,32]. As a result, the device's performance will dramatically reduce, and the Auger effect QCSE will cause significant peak changes but also cause a significant drop in luminous efficiency under high injection currents [31,33]. To mitigate this polarization field, growing quantum wells in semipolar or non-polar directions allows better overlap of electrons and holes, which leads to faster radiation recombination, especially with thicker quantum wells [34–40]. It was expected that a higher electro-optical bandwidth and potentially reduced Auger effect could be achieved by crystal orientation.

With the advantages of semipolar LEDs in luminous efficiency and wavelength stability, researchers have expanded their applications; for instance, in high-resolution displays and high-speed visible light communications. Nevertheless, better implementation of VLC includes improving the modulation characteristics of LED light sources and the emission efficiency under high-speed modulation, which depend on their carrier recombination lifetimes.

Semipolar LEDs with less QCSE have a faster radiation recombination rate [30]. However, μ -LEDs have a better frequency response, low power consumption, and higher brightness [36]. The high brightness of a μ -LED leads to a faster transmission data rate and lower bit error rate (BER). By using a high-speed photodetector to detect the modulated LED photocurrent signal, the -3 dB frequency is related to specific diode parameters. The frequency response has been evaluated using a fixed current. The LED cut-off frequency was affected by the carrier lifetime and Resistor-Capacitor (RC) time constant composed of depletion layer capacitance and the junction differential resistance, which determines the transmission data rate of the LED.

The modulation bandwidth can determine the data rate of the VLC application, so the -3 dB frequency bandwidth of LED can be related to the resistance-capacitance time constant (τ_{RC}) and the minority carrier lifetime, as shown in the Equation (1) [37]:

$$f_{-3dB} = \frac{\sqrt{3}}{2\pi\tau} = \frac{\sqrt{3}}{2\pi} \left(\frac{1}{\tau_r} + \frac{1}{\tau_{nr}} + \frac{1}{\tau_{RC}} \right) \quad (1)$$

where τ_r and τ_{nr} represent the radiative and non-radiative carrier lifetime, respectively.

The modulation bandwidth of GaN LEDs is mainly determined by the RC time constant and carrier lifetime [41–44]. The modulation bandwidth can be increased due to the decrement of the carrier lifetime by increasing the injected current density [38,45]. However, increasing the current density may cause the quantum efficiency and LED performance to decrease [46]. Several reports have indicated the carrier recombination process in GaN-based LEDs would be influenced by carrier localization [47–49] and the QCSE [50,51]. μ -LEDs can achieve a smaller carrier lifetime and higher modulation bandwidth because they can withstand higher injection current density. As the current density increases, QCSE will become less effective, increasing the optical power and modulation bandwidth [52]. Because the μ -LED has a smaller active area, the relative geometric capacitance and RC time constant, the main parameters limiting the modulation bandwidth, will be reduced. Growing LEDs on semipolar or non-polar substrates increased the modulation bandwidth, corresponding to a higher radiation recombination rate. GaN-based μ -LEDs have excellent performance in high brightness, high contrast, fast response time, extended service life, and low power consumption. Because of its ultra-small light-emitting area, a single μ -LED has a low power emission. By assembling multiple μ -LEDs into array, the output light power can be increased. A μ -LED array will be prepared for monochromatic and polychromatic

emission [53,54]. In this section, we review the characteristics and applications of μ -LED arrays in the field of VLC, and a brief benchmark for μ -LEDs used in VLC systems is shown in Figure 3 [42,55–64]. To utilize μ -LEDs in a VLC system, integrating multi-color emitters on a single chip is required. This can be achieved by combining blue μ -LEDs with color conversion materials (pc-LED) or RGB-LEDs.

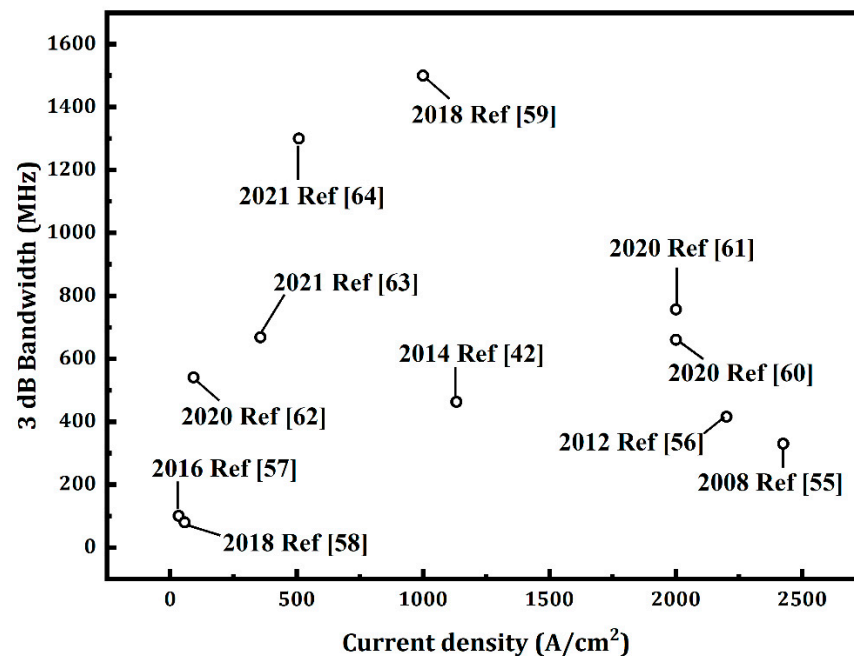


Figure 3. Benchmark for μ -LEDs used in VLC system.

2.2. Theoretical Background of Laser for VLC Application

Due to the low data transmission rate of the LED modulation, Professor Hardal Hass was the first to use laser diodes to replace LEDs for Li-Fi. By utilizing lasers' high energy and luminous efficiency, the data transmission rate can be ten times higher than LEDs. Laser lighting can produce white light through color mixing technology, similar to RGB LEDs. Although an LED-based VLC can achieve a transmission rate of 10 Gb/s and increase the upper limit of the data transmission rate of 7 Gb/s in Wi-Fi, the laser data transmission rate can easily exceed 100 Gb/s. The R&D team of Arizona State University developed a nano-scale white light laser which can be a potential Li-Fi light source. Laser diodes have several advantages in communication applications: faster response speed, direct modulation, and high coupling efficiency. For general semiconductor lasers, the LD can modulate light controlled by the input current when the injected current exceeds the threshold current (I_{th}), as the modulation characteristics show in Figure 4. The linear region above the threshold current to the saturation area is the LD working area, the modulation range. Hence, reducing the device threshold current and obtaining a more extensive modulation working area is crucial.

The threshold current density is shown in Equation (2):

$$J_{th} = \frac{ed}{I_{inj}} \left(BN'^2 e^{2\frac{\alpha_m + \alpha_i}{\Gamma_{g0}}} + CN'^3 e^{3\frac{\alpha_m + \alpha_i}{\Gamma_{g0}}} \right) \quad (2)$$

where J_{th} is threshold current density; e is the electron element charge; d is the active layer thickness; I_{inj} is the injection current; N' is the transparent carrier concentration; α_m and α_i are the mirror loss and optical absorption loss, respectively; Γ_{g0} is Maximum mode gain; and B and C are the radiation recombination coefficient and Auger recombination coefficient, respectively.

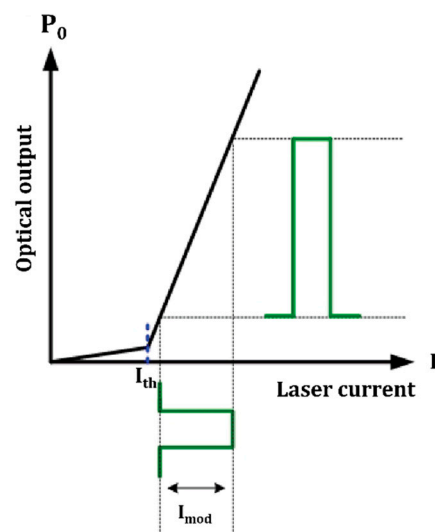


Figure 4. Laser modulation characteristics.

A laser-based VLC system reaches tens of gigabit-per-second of data rates, benefiting from its extensive modulation bandwidth. The modulation speed of the laser diode is controlled by the photon lifetime (\sim ps) rather than the carrier lifetime (\sim ns) in the LED. In addition, a laser-based VLC system enables narrow beam transmission for long-distance applications. A 100 m OOK-modulated VLC link was demonstrated with a data rate of 2.3 Gbps in 2017 [65]. While the OOK modulation technique is commonly used due to its simplicity, many advanced modulation schemes have been used in laser-based VLC to realize high data rates, with the feasibility to exceed 100 Gbps.

In a high-speed VLC system, the transmitter is critical to achieving a high data rate. A promising light source in a VLC system requires high optical output power, large modulation bandwidth, high energy conversion efficiency, low operation voltage, small form-factor, and long lifetime. Since the blue-green lasers were based on gallium nitride materials, the high-speed laser-based VLC system requires a fast GaN-based transmitter. Three types of lasers were commonly used as transmitters: edge emitting laser diodes (EELDs), super luminescent diodes (SLDs), and vertical-cavity surface-emitting lasers (VCSELs).

2.2.1. Edge Emitting Laser Diodes (EELDs)

A typical white laser transmitter is constructed using a blue laser exciting yttrium aluminum garnet (YAG) phosphor. Nakamura et al. performed the first demonstration of an InGaN/GaN-based room-temperature EELD [66], utilizing the injection locking technique and demonstrating that the bandwidth of the laser diode can be enhanced, making it promising for high data rate VLC systems [67]. In 2018, Mukhtar et al. demonstrated a prism-based self-injection locked (SIL) external cavity diode laser based on a violet LD with a continuous wavelength tunability of 5.15 nm [68]. In 2020, Holguin-Lerma et al. demonstrated that a novel InGaN-based distributed feedback (DFB) laser diode with narrow-linewidth emission at approximately 480 nm enabled a 10.5 Gbps data rate using a 16-QAM OFDM modulation scheme [69].

The phosphor material is laser-pumped to produce eye-safe white light emission, which has significant advantages over the non-human-eye-safe beam from a single-wavelength coherent emission high-power LD chip [70,71]. Figure 5 shows an integrated surface-mount device (SMD) package for laser lighting applications. The laser beam hits the phosphor, and the combination of photons from the LD and the phosphor converts the photons to produce a white light spectrum. These laser SMDs can produce a directional beam of 400–500 lumens from a 300–400-micron spot, producing a brightness level beyond 1000 cd/mm² [72].

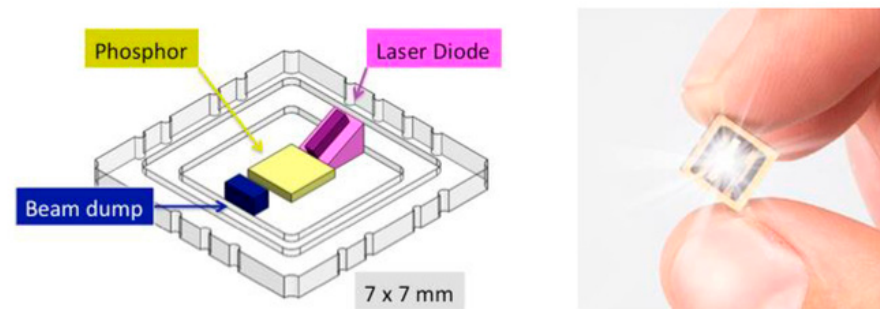


Figure 5. An integrated surface mount device (SMD) package for laser lighting applications. Figure reused from [73] with permission from SPIE.

2.2.2. Super Luminescent Diodes (SLDs)

SLDs shown in Figure 6 are light emitters generating amplified spontaneous emission (ASE), combining optical characteristics of LEDs and LDs. An SLD combines the advantage of both an LD and LED. That is, the diffraction-limited, spatially coherent, excellent coupling to external component, and small form factor of the LD, and the wideband spectrum and time incoherence of the LED [74].

Since developing high-power and high-speed violet-blue SLDs, VLC systems based on SLD transmitters have been demonstrated with data rates of 3.8 Gbps with a DMT modulation scheme by Hu, F. et al. in 2020 [75]. Studies have shown that GaN-based SLDs can achieve high power emission power, such as over 100 mW blue SLD in continuous wave operation [76].

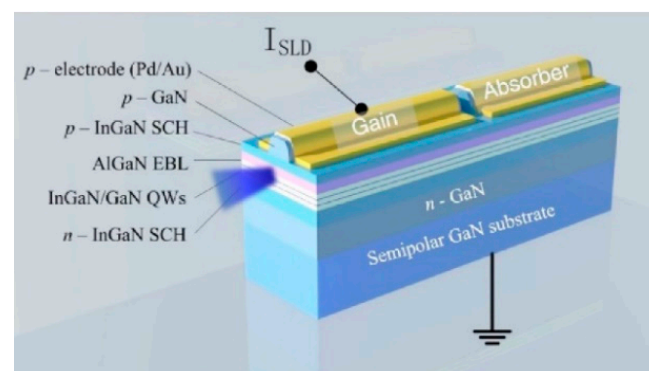


Figure 6. Schematic of a SLD [77]. © 2016 Optical Society of America.

2.2.3. Vertical Cavity Emitter Lasers (VCSELs)

VCSELs, illustrated in Figure 7, are ideal for high-speed communication systems owing to their high optical beam quality and short cavity. However, the GaN-based violet-blue-green emitting VCSELs suffer from the large lattice-mismatch AlGaIn/GaN distributed Bragg reflectors (DBRs). Research efforts are required to develop room-temperature continuous-wave operation high power GaN-based VCSELs. Experimental results have revealed the modulation bandwidth of violet-blue InGaIn/GaN quantum-well VCSEL beyond GHz, confirming that GaN-based VCSELs have great potential for high-speed VLC transmitters [78].

However, a laser diode could be a possibility for a Li-Fi light source; Nobel Laureate in Physics Nakamura Shuji anticipated that laser illumination would eventually replace LED lighting, but the current lighting technology is led by the rather established and low-cost LED. The development of high-brightness, high-efficiency, high-speed modulation micro-LED modules and laser diodes, among other features, may accelerate Li-Fi technology's commercialization. We summarize the recent research achievements in LED and laser-based VLC in Table 2.

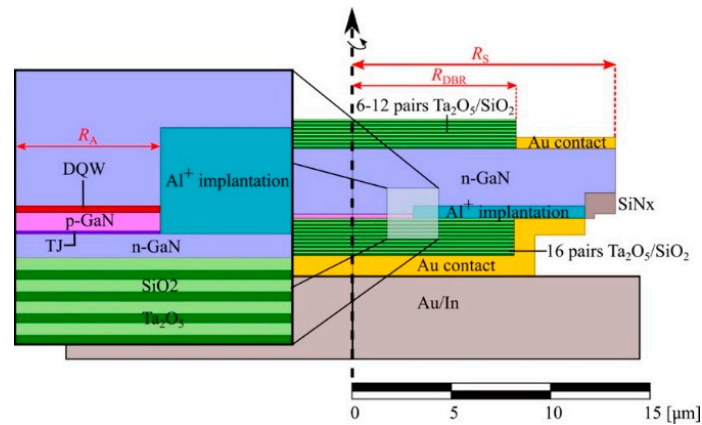


Figure 7. A schematic of a VSEL. Reprinted from [79], Copyright 2020, with permission from Elsevier.

Table 2. Recently proposed high-speed LED and LD-based VLC systems.

Light Source	Data Rate (Gbps)	Modulation Method	Distance (m)	Suitable of Lighting	Ref.
white phosphor	1.1	MIMO OFDM ¹	1	Yes	[80]
RGB LED	3.4	WDM OFDM	0.3	Maybe	[81]
RGB LED	6.36	MIMO OFDM	1	Maybe	[82]
RGB LED	3.375	PAM8	1	Maybe	[83]
RGBYC LED ²	10.72	MIMO OFDM	1	No	[84]
GaN μ -LED	5	OFDM	0.05	No	[85]
GaN violet μ -LED	11.95	OFDM	N/A	No	[86]
DUV μ -LED ³	1	OFDM	0.3	No	[87]
InGaN/GaN μ -LED	1.5	OOK	N/A	No	[61]
GaN Blue LD	2.5	OOK	0.5	No	[20]
Red VSECL	12.5	OFDM	5	No	[88]
Blue LD	9	OFDM	5	No	[22]
GaN Blue LD	4	OOK	0.15	No	[89]
Blue LD	18	OFDM	16	No	[90]
Violet LD	26.4	DMT	0.5	No	[91]
Red VSECL	11.1	OFDM	1.2	No	[92]
Red VSECL	10.6	OFDM + OOK	3	No	[93,94]
Blue LD + phosphor	4	OFDM	0.5	Yes	[24]
Blue LD + phosphor	2	OOK	1	Yes	[23]
Blue LD + phosphor	1.25	OOK	1	Yes	[95]
NUV LD + phosphor ⁴	1.25	OOK	0.15	Yes	[96]
Blue LD + phosphor	2.705	OFDM	1.5	Yes	[97]
Blue LD + phosphor	5.2	OFDM	0.6	Yes	[25]
Blue LD + phosphor	6.915	OFDM	1.5	Yes	[98]
RGB LD	8	OFDM	0.5	Maybe	[27]
RGB LD	20.231	OFDM	1	Maybe	[99]
RGBV LD ⁵	26.228	OFDM	2	Maybe	[100]

¹ MIMO: Multiple-input multiple-output. ² RGBYC LED: Red-green-blue-yellow-cyan LED. ³ DUV μ -LED: Deep-ultraviolet μ -LED. ⁴ NUV LD: Near-ultraviolet LD. ⁵ RGBV LD: Red-green-blue-violet LD.

3. VLC Receiver Technology

The following are the basic requirements of photodetectors in a visible light communication system:

1. The wavelength has a sufficiently high responsivity. For a certain incident optical power, the output photocurrent can be as large as possible.
2. Fast enough response speeds to be implemented to a high-speed broadband system.
3. A sufficiently fast response speed can be applied to high-speed broadband systems. The noise level must be as low as possible to reduce the impact on the device's signal.

4. According to a good linear relationship, the signal conversion process has been guaranteed to spread without distortion.
5. Small size and has a long service lifetime.

There are three critical parameters for photodetector: responsivity, bandwidth, and dark current [101]. Responsivity is a wavelength-dependent metric that measures the gain of an output electrical signal per unit of incident optical power incident on the detector. The responsivity, R , shown in Equation (3) where incident optical power is P , output electrical signal current is I , is usually given in amperes per watt (A/W):

$$R = \frac{I}{P} \quad (3)$$

The quantum efficiency η , which is relative to the maximum possible current, is also comparable to responsivity. When the photodetector picks up every electron-hole pair generated by the incident photons, the quantum efficiency will be denoted as 100%. Hence, Equation (3) can be rewritten into Equation (4), where q is the electron charge, λ is the wavelength of the incident light, h is the Plank constant, and c is the speed of light.

$$R = \eta \frac{q\lambda}{hc} \quad (4)$$

The bandwidth (BW) corresponds to the rise time (t_r) of the photodetector, which is shown in Equation (5):

$$BW = \frac{0.35}{t_r} \quad (5)$$

Two crucial parameters influence the bandwidth of a detector: the transit time and the RC parasitic response. Transit time is the time it takes for carriers generated by an optical signal to be swept out of the detector's active region. The velocity of the carriers is given by the following Equation (6):

$$v = \mu E \quad (6)$$

where μ is the carrier mobility and E is the electric field. When biased with a high enough electric field, the carriers will reach a saturation velocity, v_{sat} . The mobility is thus modified to be as Equation (7):

$$\mu_{sat} = \frac{\mu}{\sqrt{1 + \left(\frac{\mu E}{v_{sat}}\right)^2}} \quad (7)$$

The bandwidth is then given by Equation (8) [102]:

$$f_{transit} = 0.38 \frac{v_{sat}}{h_{PD}} \quad (8)$$

where h_{PD} is the full height of the photodetector.

Another parameter in determining the bandwidth of a detector is the electrical impedance characteristic of the detector circuit, also known as the RC parasitic response. The bandwidth due to RC limitations is shown in Equation (9):

$$f_{RC} = \frac{1}{2\pi RC} \quad (9)$$

The total bandwidth, which includes both RC and transit time effects, is given by Equation (10):

$$BW = \left(\frac{1}{f_{RC}^2} + \frac{1}{f_{transit}^2} \right)^{-1/2} \quad (10)$$

DC current may occur in the detector, even with the absence of the photons, which is known as dark current. Sufficient levels of dark current can result in a decrease in

the signal-to-noise ratio. Bulk generation and surface generation are considered when calculating the total dark current. Bulk generation is a volume-dependent mechanism in which a significant lattice mismatch between germanium and silicon causes threading dislocations, allowing for mid-bandgap states, and results mainly from the Shockley-Read-Hall process [103]. Although the bulk current density is relatively constant at a low electric field, as the electric field increases, band bending will result in a higher bulk current density that increases exponentially with the applied electric field. Surface generation is another factor that leads to dark current, and results from surface defects such as dangling bonds. Surface passivation is more difficult with germanium than silicon as germanium is not fully passivated by silicon dioxide. Other materials such as germanium oxide have been used for passivation with some success [104].

The total dark current is given by Equation (11):

$$I_{dark} = J_{bulk}A + J_{surf}\sqrt{4\pi}\sqrt{A} \quad (11)$$

where A is the junction area. Suppose we assume that bulk current dominates; then, the dark current scales with detector area. There is an approximately linear increase of dark current with the area of the detector.

The shot noise is usually the dominant noise factor in germanium on silicon photodetectors. The shot noise due to the dark current is given by Equation (12):

$$I_n = \sqrt{2qI_{dark}BW} \quad (12)$$

The avalanche photodiode (APD), PIN photodetector, metal-semiconductor-metal photodetector (MSM-PD), superlattice avalanche photodetector (SL-APD), waveguide photodetector (WGPD), and cavity-enhanced photodetector (CE-PD), are the most used photodetectors in optical communications. The free-space VLC receiver with large-area APD has a -3 dB modulation bandwidth of 420 MHz [105]. With a data rate of 56 Mbps, triple cationic perovskite solar cells can also be used as VLC receivers [106].

The bandwidth is limited by the RC time constant in the perovskite solar cell receiver. A high-performance surface-absorbing semipolar InGaN/GaN PIN-based micro-PD demo a -3 dB modulation bandwidth of 347 MHz, suggesting its promising performance for VLC applications [107]. A black silicon photodetector is developed that shows high gain in the visible-NIR regime (400–1200 nm). A high responsivity of 1097.60 A/W at 1080 nm is reported, indicating its advantages for weak light detection. Table 3 summarizes the recent research achievements in receiver technology for VLC.

Table 3. Recently proposed receiver for VLC system.

Year	Receiver Type	Bandwidth (MHz)	Data Rate (Gbps)	Responsivity (A/W)	Chip Material	Ref.
2018	PD	0.82	N/A	1.2 ¹	Triple-cation perovskite	[108]
2019	scintillating-fibers photoreceiver	86.13	0.25 (OOK)	N/A	N/A	[109]
2019	SL-APD	N/A	0.5 (PAM4)	N/A	silicon	[110]
2019	APD	155	N/A	0.35 ²	silicon	[105]
2020	Micro-PD	300	7.4 (OFDM)	0.11 ³	Semipolar InGaN/GaN PIN	[111]
2020	PD	Rise/fall time: 0.65/2.13 ms		~100 ³	Black silicon	[112]
2020	Micro-PD	347	1.55 (OOK)	0.191 ³	Semipolar InGaN/GaN PIN	[107]
2020	Solar cell	0.114~0.586	0.056 (DCO-OFDM)	N/A	Triple-cation perovskite	[106]
2021	APD	890	2 (OOK)	0.45 ⁴	silicon	[113]

¹ At 500 nm; ² at 450 nm; ³ at 400 nm; ⁴ at 675 nm.

4. Modulation Technology in VLC System

Due to the low bandwidth of the light-emitting diodes (LEDs) used in visible light communication (VLC), complex modulation schemes are a potentially attractive approach to offer high-speed data transmission. Different from other types of communication, the modulation scheme of VLC must achieve a higher rate and meet the requirements of human perception of light. The following two attributes can characterize these requirements for perceiving light.

- Dimming:

Performing different types of activities that require different levels of illuminance. For example, the illuminance in the range of 30–100 lux is sufficient to perform simple visual tasks in most public places. If the LED can be adjusted to any level, it is necessary to understand the impact of human perception of light, meaning that the human eye expands to adapt to a lower illuminance at the pupil to allow more light to enter the eye. The characteristics of the perceived light of the human eye are shown in Figure 8.

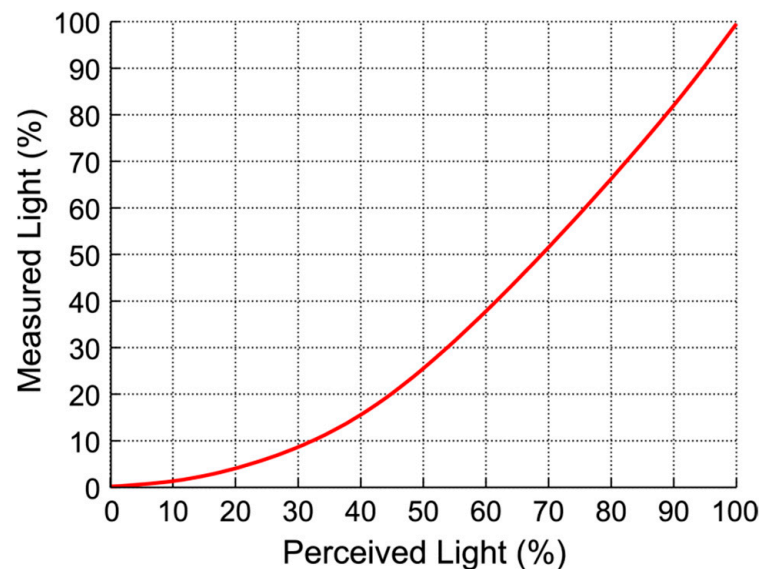


Figure 8. Human eye perceives the actual light differently due to enlargement/contraction of pupil. © 2015 IEEE. Reprinted, with permission from [114].

- Flicker reduction:

The VLC modulation scheme requires that humans should not perceive the brightness of the flicker. The flicker can cause harmful and severe physiological changes in the human body, as shown in [115]. Therefore, it is necessary to change the light intensity faster than the human eye can perceive the flicker or change the light intensity faster than 200 Hz to avoid any harmful effects, according to the IEEE 802.15.7 standard [116]. This means that the VLC Modulation scheme should reduce flicker while providing a higher data rate.

After preprocessing, encoding and modulation, a binary bitstream drives the LD (or LED), and the electrical signal implemented the intensity modulation to convert into an optical signal. Each modulation technique has a finite number of symbols in which data can be encoded. Having more symbols allows the representation of more bits by a single symbol. For example, if an eight-symbol modulation technique is used, each symbol can represent a set of three bits because each set can have one of eight possibilities. In general, each symbol of an M-symbol scheme can represent $k \frac{1}{4} \log_2 M$ bits, and these k bits are mapped such that adjacent symbols differ by only one bit (gray encoding). Therefore, the incorrect selection of adjacent symbols results in a single bit error. However, the use of such techniques comes with an increase in the power required or a decrease in the immunity of error.

The five common modulation schemes of VLC are:

1. Multilevel pulse amplitude modulation (M-PAM)
2. Phase shift keying (PSK) modulation
3. M-ary quadrature amplitude modulation (M-QAM)
4. Orthogonal frequency division modulation (OFDM)
5. Color shift keying (CSK) modulation

4.1. Multilevel Pulse Amplitude Modulation (M-PAM) Technique

Multilevel pulse amplitude modulation (M-PAM) is a conventional multilevel modulation scheme and is the generalization of non-return-to-zero (NRZ) on-off keying (OOK) from a set of two symbols to a set of M symbols, as illustrated in Figure 9. For example, when the LED/Laser is turned off, the light intensity will not be completely switched off, but the optical intensity will be diminished. Where $Q(\cdot)$ is the Q function, the BER and SNR relation of M-PAM can be determined by Equation (13) [117]:

$$BER_{M-PAM} = \frac{M-1}{M} \frac{2}{\log_2 M} Q\left(\frac{\sqrt{SNR}}{M-1}\right) \quad (13)$$

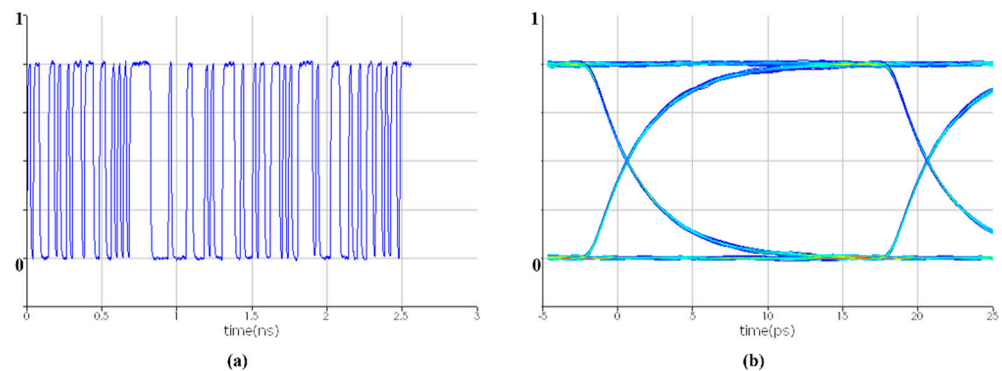


Figure 9. The (a) V-t diagram and (b) eye diagram of a pseudo-random binary sequence (PRBS) OOK signal.

4.2. Phase Shift Keying (PSK) Modulation Technique

Phase shift keying (PSK) is a digital modulation scheme that conveys data by changing, or modulating, the phase of a reference signal (the carrier wave). Although Binary-PSK (BPSK) is the simplest form of PSK, which uses two phases separated by 180° , it can only modulate at 1 bit/symbol. The motivation behind M-ary PSK (MPSK) is to increase the bandwidth efficiency of the PSK modulation scheme. Figure 10 illustrated the constellation diagrams for BPSK, QPSK and 8PSK. Gray encoding was also used to map the sets of bits to the appropriate symbol. Where $erfc(\cdot)$ is the error function, the BER and SNR relation of BPSK and QPSK can be determined by Equations (14) and (15) [118], respectively:

$$BER_{BPSK} = \frac{1}{2} erfc(\sqrt{SNR}) \quad (14)$$

$$BER_{BPSK} = erfc(\sqrt{SNR}) = 2BER_{BPSK} \quad (15)$$

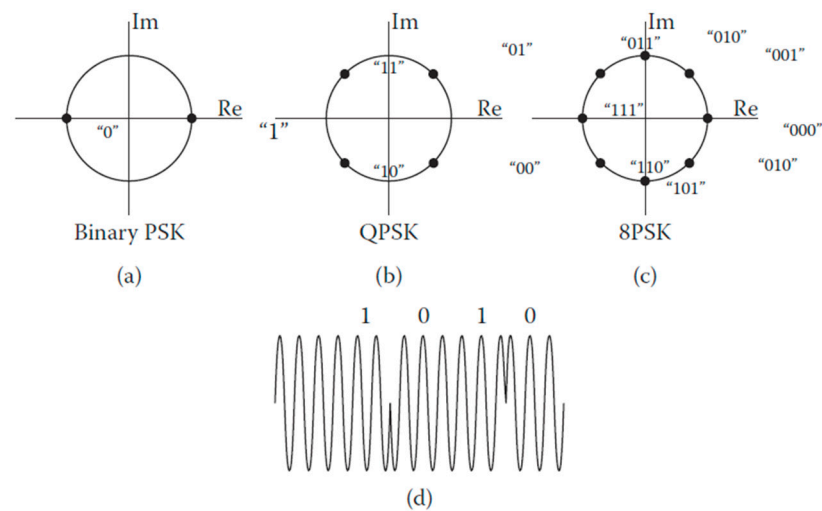


Figure 10. Signal-space constellation of discrete PM: (a) binary PSK, (b) quadrature binary PSK, (c) eight PSK and (d) phase of the carrier under modulation with π phase shift of the BPSK at the edge of the pulse period. From: [119], Copyright © 2015 and Imprint. Reproduced by permission of Taylor & Francis Group through PLSclear.

4.3. M-Ary Quadrature Amplitude Modulation (QAM) Technique

QAM combines both PSK and amplitude-shift keying by changing the two parameters of the carrier. For that reason, this method is also known as amplitude phase keying [120]. With the same average signal strength, the number of symbols can be raised to represent more bits by a single symbol, resulting in improved bandwidth efficiency compared to MPSK. The constellation diagrams of 8-QAM and 16-QAM are shown in Figure 11. The BER and SNR relation of M-QAM can be determined by Equation (16) [121]:

$$BER_{M-QAM} \cong \frac{\sqrt{M}-1}{\sqrt{M}} \frac{4}{\log_2 M} Q\left(\sqrt{\frac{3}{M-1} SNR}\right) \quad (16)$$

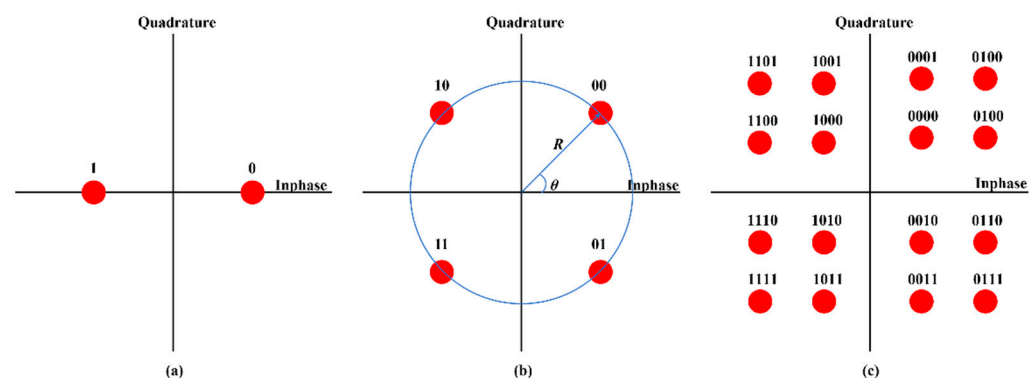


Figure 11. Constellation diagram of (a) BPSK, (b) 4-QAM (QPSK) and (c) 16-QAM.

4.4. Orthogonal Frequency Division Modulation (OFDM) Technique

OFDM uses multiple subcarriers with orthogonal frequencies to utilize the available bandwidth efficiently. The OFDM diagram transmission and reception is shown in Figure 12 [119]. The serial data stream is converted to a parallel stream and mapped using a modulation scheme, such as PSK or QAM. The data flow is then imposed with Hermite symmetry to ensure that the inverse fast Fourier transform (IFFT) output in the following block is true valued. The use of PSK or QAM is therefore possible when OFDM is employed. If the size of the IFFT is N, N/2 symbols going into the IFFT will represent the data to be transmitted, and the other N/2 symbols will be their conjugates. This ensures that the IFFT

generates only real values. The analytical expression between the BER and SNR of M-QAM OFDM can be determined by Equation (17) [122]:

$$BER = \frac{4\sqrt{M} - 1}{\sqrt{M} \log_2(M)} Q\left(\sqrt{\frac{3 \log_2(M)}{M-1}} SNR\right) + \frac{4\sqrt{M} - 2}{\sqrt{M} \log_2(M)} Q\left(3\sqrt{\frac{3 \log_2(M)}{M-1}} SNR\right) \quad (17)$$

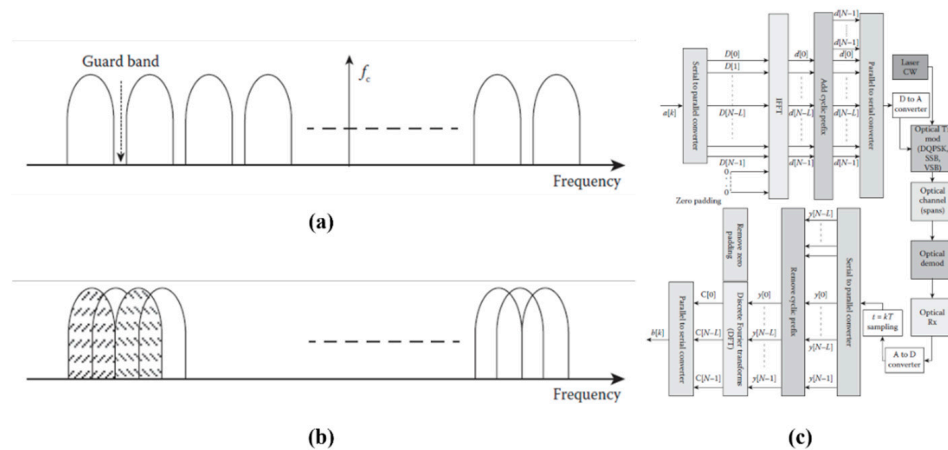


Figure 12. Spectrum of multicarrier modulation scheme (a) frequency division multiplexing and (b) OFDM, (c) a block diagram of OFDM system using N-point FFT and IFFT. From: [119], Copyright © 2015 and Imprint. Reproduced by permission of Taylor & Francis Group through PLSclear.

4.5. Color Shift Keying (CSK) Modulation Technique

The blue LED chip excites the yellow phosphor to produce white light, but its switching speed capability slows down. Therefore, green, blue, and red are used to achieve white light through light mixing technology. CSK is mentioned in IEEE 802.15.7 and lower data rate is used in other modulation schemes [123]. The modulation of CSK is performed using the intensities of the three colors of RGB LED. CSK is sampled in the color space chromaticity diagram [114]. It maps the eye-perceivable color to two chromaticity factors, x and y . Table 4 illustrates the seven bands of human-visible wavelengths, the centers of which are marked in Figure 13. Where k is the number of bits ($k = \log_2 M$), M is the modulation order and N_0 is one-sided noise power spectral density, the bit error probability (BEP) of a 4-CSK three color LEDs (Trichromatic LEDs, TLED) can be determined by Equation (18) [124]:

$$BEP_{4-CSK} = \frac{1}{2k} Q\left(\frac{0.8157}{\sqrt{2N_0}}\right) + \frac{1}{2k} Q\left(\frac{0.817}{\sqrt{2N_0}}\right) \quad (18)$$

Table 4. CSK in code and chromaticity coordinates. © 2015 IEEE. Reprinted, with permission, from [114].

Wavelength (nm)	Code	Center (nm)	(x, y)
380~478	000	429	(0.169, 0.007)
478~540	001	509	(0.011, 0.733)
540~588	010	564	(0.402, 0.597)
588~633	011	611	(0.669, 0.331)
633~679	100	656	(0.739, 0.271)
679~726	101	703	(0.734, 0.265)
726~780	110	753	(0.734, 0.265)

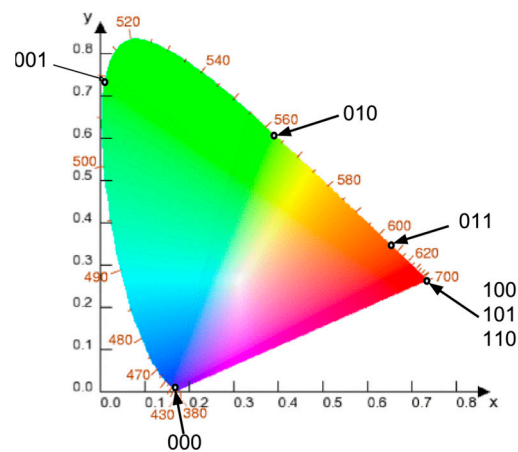


Figure 13. Chromaticity diagram. © 2015 IEEE. Reprinted, with permission from [114].

4.6. Power Requirements and Spectrum Efficiency

The power requirement for an OWC system is proportional to the square root of the SNR, as shown in Equation (19) [117]:

$$P = \frac{1}{R} \sqrt{\sigma_N^2 SNR} \tag{19}$$

where R is the responsivity of the photodetector and σ_N^2 is the total noise power in the detector current.

Hence the normalized average power requirement of M-PAM, BPSK, QPSK is shown in Equations (20)–(22), respectively:

$$\frac{P_{M-PAM}}{P_{NRZ-OOK}} = \frac{M - 1}{\sqrt{\log_2 M}} \tag{20}$$

$$\frac{P_{BPSK}}{P_{NRZ-OOK}} = \frac{1}{2\sqrt{2}} \tag{21}$$

$$\frac{P_{QPSK}}{P_{NRZ-OOK}} = \frac{1}{2\sqrt{2}} \frac{\text{erfc}^{-1}(BER)}{\text{erfc}^{-1}(2BER)} \tag{22}$$

Nowadays, the most commonly used modulation schemes are the M-QAM OFDM, NRZ-OOK, and M-PAM. Among them, M-PAM has better spectral efficiency but requires higher SNR to maintain targeted BER, as illustrated in Figure 14.

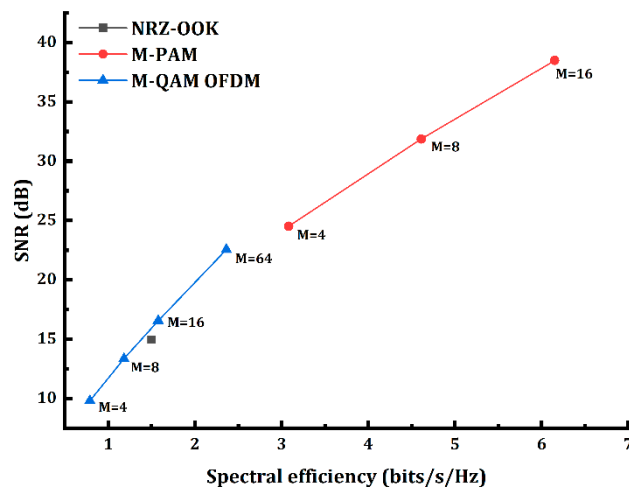


Figure 14. Spectral efficiency vs. SNR requirement for a BER of 10^{-3} .

5. Optical Wireless Communication Standards

VLC is the most promising technology for communications. Due to LED lighting's rapid development, the cost is rapidly falling; however, some of the challenges that must be addressed are listed as follows:

1. Integration of VLC system with existing communication standards.
2. Ambient light source interference problem.
3. VLC should properly consider mobility issues such as handover.
4. Specification of a forward error correction plan to improve communication system performance.

As the number of VLC devices increases, there will be interference between different VLC devices. The Electronic Information Technology Industry Association developed the standard 802.15.7, which is a standard established by the IEEE for the physical layer and the MAC layer [123]. Objectives of this standard are:

1. Establish access to hundreds of terahertz frequency bands.
2. Establish anti-electromagnetic interference capability.
3. Communication of additional services that supplement the current visible light equipment.
4. VLC communication that specifies a forward error correction (FEC) scheme, modulation form, and transmission rate.
5. Channel access mechanism, as visibility support also describes channel access, and contention access period (CAP) and contention-free period (CFP).
6. Physical layer specifications, such as optical mapping, TX-RX, RX-TX turnaround time, flicker, and dimming relief. IEEE 802.15.7 is new product development standard.

Three different types of devices used by VLC are vehicles, mobile equipment, and infrastructure, as shown in Table 5 [125].

Table 5. Classification of IEEE 802.15.7 devices.

	Mobile	Vehicle	Infrastructure
Fixed coordinator	No	No	Yes
Power supply	Limited	Moderate	Ample
Form factor	Constrained	Unconstrained	Unconstrained
Light source	Weak	Intense	Intense
Physical mobility	Yes	Yes	No
Range	Short	Long	Short/Long
Data rate	High	Low	High/Low

6. VLC Application

VLC provides many applications from high-speed internet chains with LED bulbs to interplanetary communication and quantum communication. VLC also brings a new perspective to computing that is considered ubiquitous. In this section, we discuss the potential of visible light communications, focusing on these applications: indoor VLC [2,10,12,88], ID and position systems [6,126], in-vehicle communications [127], and underwater communication [6,128].

6.1. Li-Fi

Li-Fi is similar to Wi-Fi, but it is a bidirectional, visible light wireless communication system. In 2011, Harald Haas first created Light Fidelity (Li-Fi). Wi-Fi signals have the problem of interference with other radio signals, such as interfering with the airplane navigation equipment. Hence, Li-Fi can be a better solution in areas sensitive to electromagnetic radiation, such as airplanes and hospitals, which is illustrated in Figure 15.



Figure 15. LiFi application in an airplane cabin. Reprinted from [28], Copyright 2019, with permission from Elsevier.

6.2. Vehicle to Vehicle Communication

Front-end collision warning, pre-collision sensing, emergency stop lights, lane change warning, parking movement assistance, left turn assist, signal violation warning, and corner speed limit warning are among the most important vehicle safety communication initiatives [129]. A Li-Fi high-speed visible light communication system can be employed for these, since all high-priority applications require extremely low latency reachability and the permissible delay of vehicle safety communication is ultra-low.

6.3. Underwater Communication

Due to the extremely high attenuation of radio frequency waves in water, RF or near-infrared OWC cannot propagate well in sea water [130]. Therefore, an underwater communication (UWOC) network should adopt VLC communication as shown in Figure 16.

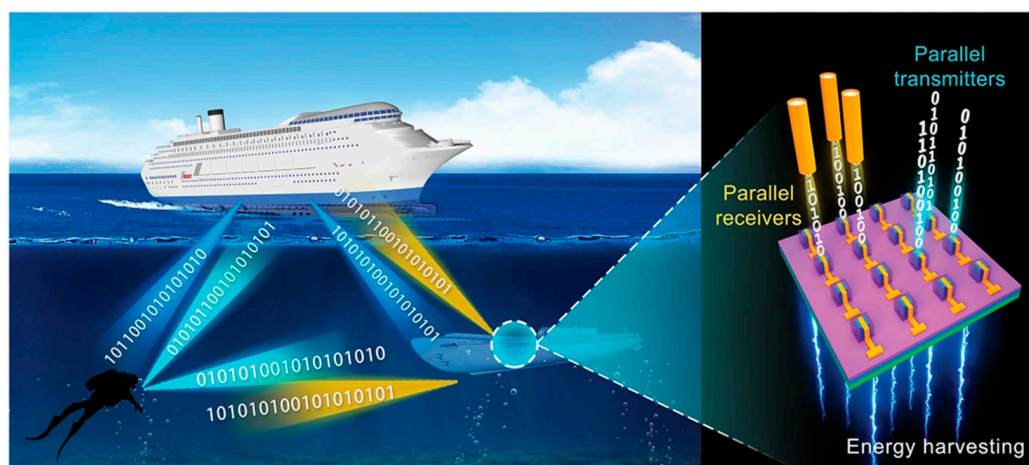


Figure 16. Illustration of application scenarios of duplex UWOC and charging technologies based on a micro-LED array [131]. Figure reused with permission from John Wiley and Sons.

For underwater application, the attenuation of the light can be evaluated through Equation (23) [132]:

$$P_d = P_0 e^{-c(\lambda)d} \quad (23)$$

where P_0 is the output power of the light source, P_d is the received power over certain distance d , and $c(\lambda)$ is coefficient of water associated with attenuation. By evaluating Equation (23) and by assuming the output power to be 1 mW we can obtain the propagation

distance of visible light in ocean water, as illustrated in Figure 17. In clear ocean water, blue and green light are usually preferable to red light, as illustrated in Figure 17a; however, the attenuation and scattering of red light are lower for certain environments such as a highly turbid harbor [133], as illustrated in Figure 17b.

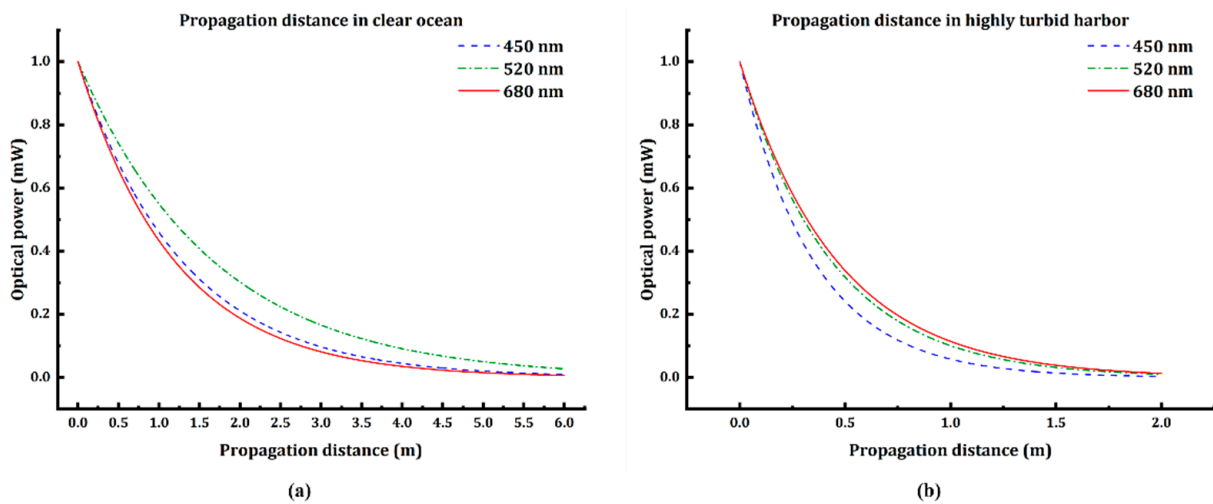


Figure 17. The propagation distance of different wavelengths in (a) clear ocean water, (b) a highly turbid harbor.

6.4. Information Displaying Signboards

LEDs are utilized as light sources on signboards set in a specific order at airfields, bus stations, and other locations where information must be broadcasted. In venues such as airports, museums, and hospitals, signs are utilized to transfer data and can also be used for instructions [134], as shown in Figure 18.

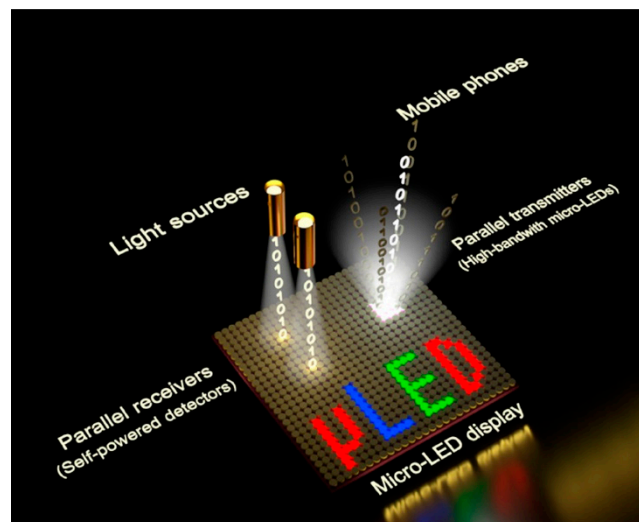


Figure 18. VLC using in information displaying signboards. Reprinted with permission from [135]. Copyright 2019, American Chemical Society.

6.5. Visible Light ID and Position System

Visible light can be used as an identification system and to determine indoor position, similar to a global position system (GPS). For instance, if we were standing in room 15 of a certain building, the system could be used to identify the room number and its building [6,126].

6.6. Wireless Local Area Networks (WLANs)

In Figure 19, an ultra-high-speed full-duplex local area network with star topology is shown, with LED visible light communication set up for the LAN, using VLC to provide speeds exceeding 10 Gb/s, and is tested by a large number of users.

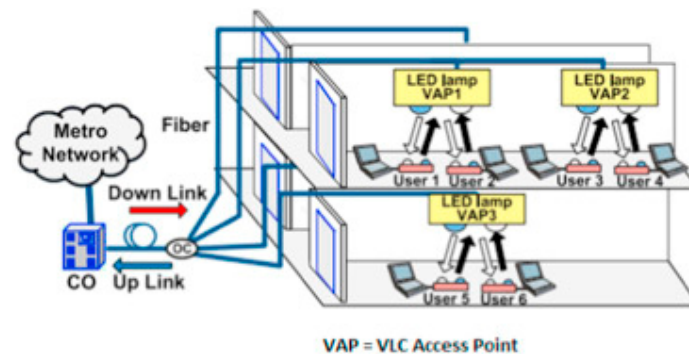


Figure 19. VLC using in wireless local area networks. Figure reused from [5] under a Creative Commons Attribution Non-commercial Non-Derivative 4.0 International license (CC BY-NC-ND 4.0).

7. Challenges

While VLC has many advantages over RF communication, it also faces unprecedented challenges that need to be mitigated. One of these challenges is commercialization, in which lighting companies and phone manufacturers have to develop their future devices to accommodate the current VLC technologies for use in future applications. Another challenge is creating new VLC standards and developing the current ones by considering the latest technological evolutions in the field [126]. In addition, the performance of VLC can be degraded or distorted due to background noise. Manchester coding mitigates this background noise [6]. Moreover, to cater for dual-functionality LD- or SLD-based SSL-VLC applications, the quality of the produced white light still needs to be improved using stable light converters that can be used for prolonged periods of time. The use of LDs as data transmitters also faces issues with misalignment and outages because there are many ways in which the line-of-sight link between the transmitter and the receiver might be lost or blocked. A critical concern is the hazards related to eye safety, as long-term exposure to high-intensity light is potentially harmful to human vision and circadian rhythm. In the case of using conventional LEDs as transmitters, the limitation in allowable bandwidths would potentially limit the transmission rate in Li-Fi systems; thus, micro-LEDs and LDs are more promising alternatives, offering higher bandwidths and transmission rates. Another updated modulation technology, quantum communication, which is also being applied to the VLC system, will introduce the principle of quantum communication.

The following section discussed the state of the art of OWC systems and potential techniques for improving the performance or the data rate. The possible solutions for solving problems of the current VLC system mention in [136] are discussed, such as:

1. Bandwidth limitation of the light source.
2. Si-based detectors are mainly sensitive to infrared waves.
3. Point-to-Point communication based on a single transmitter and detector.
4. Transmission and reception antennas require a large lens group.

7.1. Bandwidth Limitation of the Light Source

Since the limited bandwidth suppressed the speed of the VLC systems, in 2020, Huang Chen et al. successfully demonstrated a semipolar (20–21) 525 nm μ -LED that achieved 3 dB bandwidth up to 756 MHz and 1.5 Gbit/s under a current density of 2.0 kA/cm², through several improved approaches on epitaxy and chip processes, such as the introduction of atomic layer deposition (ALD) [61]. Furthermore, in 2021, Gong-Ru Lin et al. achieved beyond 5 Gbit/s OWC with a 2×2 high-contrast grating (HCG) green

μ -LED operated under low current density, decreasing the power consumption of the transmission system [137].

7.2. Si-Based Detectors Are Mainly Sensitive to Infrared Waves

In 2020, Huang et al. demonstrated a black silicon-based photodetector with high responsivity up to 100 A/W at 400 nm and broad response spectrum from 400 to 1600 nm. In their work, the broad-bandgap responsivity and SNR increase, and the dark current, are mitigated through the utilization of rapid thermal annealing and hydrogenated surface passivation [112], which may be a promising candidate for Si-based detectors for VLC systems.

7.3. Point-to-Point Communication Based on a Single Transmitter and Detector

Multiple light sources are needed to accomplish uniform lighting and elevate the data rate in a mesh multiple-point network. Nevertheless, spatial multiplexing (SMP) is the most commonly used MIMO scheme that is restricted by channel correlation, causing difficulties for receivers to distinguish a single data stream. In 2020, a novel odd-order 32-QAM constellation scheme for 2×2 MIMO VLC systems by superposing two independent signals modulated with 4-QAM and 8-QAM was illustrated by Guo et al. as a promising candidate for mitigating the channel correlation of SMP MIMO VLC system [138].

7.4. Transmission and Reception Antennas Require a Large Lens Group

This problem could be solved via the combination of a Fresnel lens and an optical antenna that is capable of radiating directionally and switching to wide-angle rapidly. In 2018, Sabouri et al. proposed a SiN-based optical phase antenna (OPA); the performance of such a design is estimated to have a $\pm 12.7^\circ$ beam steering in Azimuth angle, 15.6° in polar angle using wavelength tuning in a range of 60 nm [139]. OPA is a promising candidate due to the advantages of its small size, light-weight, rapid switching speed, and multi-beam steering [140].

8. Quantum Communication

Quantum communication is a way to transfer quantum states from the transmitter (Alice) to the receiver (Bob). Quantum Key Distribution (QKD) is a well-known case of quantum cryptography, first proposed by Bennett and Brassard in 1984 [141,142], also known as the BB84 protocol, and was first experimentally demonstrated in 1991 [143]. Different photon states, such as polarization, period, frequency, phase, and space, can realize various QKD protocols. The essence of BB84 is to pressure eavesdropper (Eve) to perform a quantum measurement that will expose her existence, by sending a series of individual photons to Bob; many of the photons never arrive or are not detected. Of the resulting bits, some are kept and used as key material, the remaining are used to hunt for Eve.

A schematic of a polarization-based BB84 QKD protocol and the four polarization states that were applied are shown in Figure 20. A polarization-based BB84 QKD protocol is often used in free-space optical (FSO), since when used over optical fiber the polarization-dependent loss, polarization mode dispersion, and the fiber loss restricted the transmission distance [144]. The beam steering system allows Alice to direct the beam to Bob without physically moving the system, and can be realized by a liquid crystal spatial light modulator (LC-SLM), LCoS-SLM, and micro-electromechanical systems (MEMs) [7,145]. The single photon source required by the BB84 protocol is realized by a high attenuation laser, which can generate weak coherent state (WCS) pulses [146].

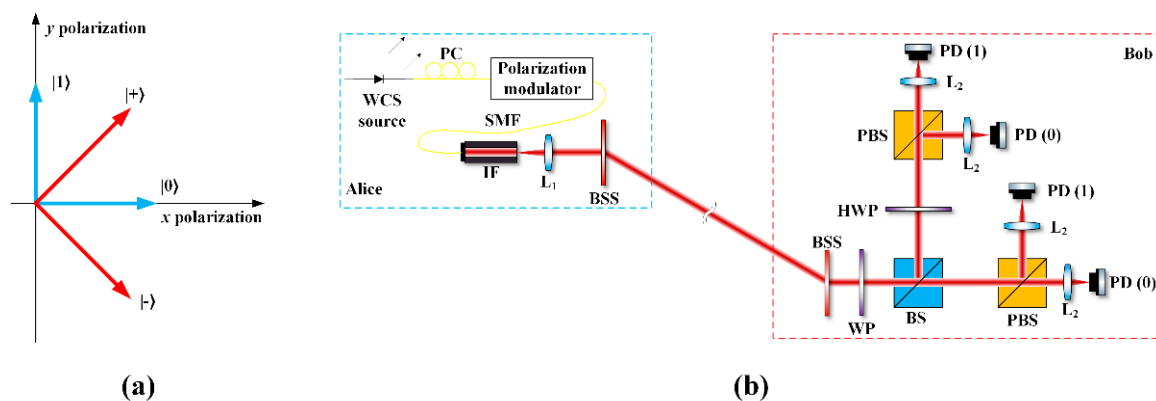


Figure 20. (a) The four states that applied and (b) the schematic of a polarization based BB84 protocol. (WCS source: weak coherent state source; PC: polarization controller; SMF: single mode fiber; IF: input fiber; L1: collimator; BSS: beam steering system; WP: wave plate; HWP: half-wave plate; BS: beam splitter; PBS: polarization beam splitter; L2: focusing lens; PD: photodetector).

The weak coherent state output by the highly attenuated laser source can guarantee that the coherent state has a high probability that there is no more than one photon. The number state $|n\rangle$ can be expressed in terms of the ground state ($|0\rangle$) with the creation operator by Equation (24):

$$|n\rangle = \frac{(a^\dagger)^n |0\rangle}{(n!)^{1/2}} \quad (24)$$

where a is the annihilation operator. The density operator of a coherent state is given by Equation (25):

$$\rho = |\alpha\rangle\langle\alpha| = e^{-|\alpha|^2} \sum_{n=0}^{+\infty} \sum_{m=0}^{+\infty} (n!)^{-1/2} (m!)^{-1/2} \alpha^n (\alpha^*)^m |a\rangle\langle m| \quad (25)$$

where a is a complex eigenvalue of the annihilation operator, and $|\alpha\rangle$ is the coherent state vector. The probability that n -photons can be found in coherent state $|\alpha\rangle$ follows the Poisson distribution shown in Equation (26):

$$P(n) = |\langle n|\alpha\rangle|^2 = e^{-\mu} \frac{\mu^n}{n!} \quad (26)$$

where $\mu = |\alpha|^2$ is the photon number. Considering that the chance of more than one photon is sent is not zero, by applying a photon number splitting (PNS) attack, it is possible for Eve to obtain information. To solve the problem above, Hoi-Kwong Lo et al. proposed a decoy-state-based quantum key distribution in 2005 [147]. In decoy-state QKD, Alice and Bob can detect whether Eve is capturing photons when more than one photon is sent since the average number of photons sent is increased during random timeslots.

The quantum mechanics laws guarantee QKD's security. According to the method utilized on Bob's side, there are two common QKD schemes: discrete variable (DV)-QKD and continuous variable (CV)-QKD, which utilize a single-photon detector (SPD) and homodyne/heterodyne detection to measure field quadrature on Bob's side, respectively. Different QKD schemes can also be classified as entanglement assist or preparation and measurement types. For DV-QKD, the unclonability theorem and in distinguishability theorem of arbitrary quantum states make absolute security possible. The unclonability theorem declares that any quantum state is unique and cannot be copied, which means that even with the help of the most powerful computer in the world, Eve cannot clone a non-orthogonal quantum state [148]. Furthermore, the distinguishability theorem states that non-orthogonal states cannot be distinguished clearly. That is to say, it is inevitable that constancy of the quantum states will be disturbed when Eve is attempting to gain

information on transmitted bits and this will be detected by Bob. The CV-QKD applies the uncertainty principle and states that the in-phase and quadrature components of the coherent state cannot be measured completely and accurately at the same time. Recently, the development of QKD has greatly improved not only theoretically but also experimentally; an LED-based decoy-state QKD was proposed recently by Jian-Wei Pan et al. in 2019 [146]. By replacing the WCS laser source with an LED, they lower the cost of the QKD system, providing a tolerable price and sufficient security.

9. Conclusions

Here, we present the recent advances in high-speed visible light communication: transmitter, modulation technology, receiver standard, and application. Micro-LED/laser-diode-based VLC are promising approaches towards next-generation wireless data communication networks, which have caught the attention of both academia and industry. VLC technology provides many advantages over RF and has become an alternative to RF communication, despite the disadvantage of blind spots due to light spacing and line-of-sight blocking. The successful development of the VLC system addresses the immediate multi-billion-dollar markets in beyond-5G optical wireless communication. Empowering the Internet of Underwater and Underground things (IoU2T), VLC will unfold many new ideas and enable future applications related to energy, connectivity, and the environment.

Author Contributions: Supervision, W.-B.L., S.-W.C., C.-W.C. and H.-C.K.; writing—original draft, T.-C.Y. and W.-T.H.; Writing—Review & editing, C.-W.C. All authors have read and agreed to the published version of the manuscript.

Funding: This research was funded by Ministry of Science and Technology, Taiwan, grant number 110-2124-M-A49-003-, 108-2221-E-009-113-MY3.

Conflicts of Interest: The authors declare no conflict of interest.

References

1. Karunatilaka, D.; Zafar, F.; Kalavally, V.; Parthiban, R. LED Based Indoor Visible Light Communications: State of the Art. *IEEE Commun. Surv. Tutor.* **2015**, *17*, 1649–1678. [[CrossRef](#)]
2. Hussain, B.; Li, X.; Che, F.; Yue, C.P.; Wu, L. Visible Light Communication System Design and Link Budget Analysis. *J. Lightwave Technol.* **2015**, *33*, 5201–5209. [[CrossRef](#)]
3. Ismail, S.N.; Salih, M.H. A review of visible light communication (VLC) technology. *AIP Conf. Proc.* **2020**, *2213*, 020289. [[CrossRef](#)]
4. Sindhubala, K.; Vijayalakshmi, B. Design and implementation of visible light communication system in indoor environment. *ARPJ. Eng. Appl. Sci.* **2015**, *10*, 2882–2886.
5. Khan, L.U. Visible light communication: Applications, architecture, standardization and research challenges. *Digit. Commun. Netw.* **2017**, *3*, 78–88. [[CrossRef](#)]
6. Zhuang, Y.; Hua, L.; Qi, L.; Yang, J.; Cao, P.; Cao, Y.; Wu, Y.; Thompson, J.; Haas, H. A Survey of Positioning Systems Using Visible LED Lights. *IEEE Commun. Surv. Tutor.* **2018**, *20*, 1963–1988. [[CrossRef](#)]
7. Chou, H.-H.; Huang, W.-T. Asymmetrical bidirectional optical wireless communication system based on a transmissive 1D LC-SLM for NG-PON2. *Opt. Lett.* **2020**, *45*, 4543–4546. [[CrossRef](#)]
8. Muthu, S.; Schuurmans, F.J.; Pashley, M.D. Red, green, and blue LEDs for white light illumination. *IEEE J. Sel. Top. Quantum Electron.* **2002**, *8*, 333–338. [[CrossRef](#)]
9. Qu, X.; Wong, S.; Tse, C.K. Temperature Measurement Technique for Stabilizing the Light Output of RGB LED Lamps. *IEEE Trans. Instrum. Meas.* **2010**, *59*, 661–670. [[CrossRef](#)]
10. Minh, H.L.; Brien, D.O.; Faulkner, G.; Zeng, L.; Lee, K.; Jung, D.; Oh, Y.; Won, E.T. 100-Mb/s NRZ Visible Light Communications Using a Postequalized White LED. *IEEE Photonics Technol. Lett.* **2009**, *21*, 1063–1065. [[CrossRef](#)]
11. Yeh, C.-H.; Liu, Y.-L.; Chow, C.-W. Real-time white-light phosphor-LED visible light communication (VLC) with compact size. *Opt. Express* **2013**, *21*, 26192–26197. [[CrossRef](#)]
12. Vučić, J.; Kottke, C.; Nerreter, S.; Langer, K.-D.; Walewski, J.W. 513 Mbit/s Visible Light Communications Link Based on DMT-Modulation of a White LED. *J. Lightwave Technol.* **2010**, *28*, 3512–3518. [[CrossRef](#)]
13. Khalid, A.M.; Cossu, G.; Corsini, R.; Choudhury, P.; Ciaramella, E. 1-Gb/s Transmission Over a Phosphorescent White LED by Using Rate-Adaptive Discrete Multitone Modulation. *IEEE Photonics J.* **2012**, *4*, 1465–1473. [[CrossRef](#)]
14. Wu, F.M.; Lin, C.T.; Wei, C.C.; Chen, C.W.; Chen, Z.Y.; Huang, H.T.; Chi, S. Performance Comparison of OFDM Signal and CAP Signal Over High Capacity RGB-LED-Based WDM Visible Light Communication. *IEEE Photonics J.* **2013**, *5*, 7901507. [[CrossRef](#)]

15. Green, R.P.; McKendry, J.J.D.; Massoubre, D.; Gu, E.; Dawson, M.D.; Kelly, A.E. Modulation bandwidth studies of recombination processes in blue and green InGaN quantum well micro-light-emitting diodes. *Appl. Phys. Lett.* **2013**, *102*, 091103. [[CrossRef](#)]
16. Dai, L.; Zhang, B.; Lin, J.Y.; Jiang, H.X. Comparison of optical transitions in InGaN quantum well structures and microdisks. *J. Appl. Phys.* **2001**, *89*, 4951–4954. [[CrossRef](#)]
17. Choi, H.W.; Jeon, C.W.; Dawson, M.D.; Edwards, P.R.; Martin, R.W.; Tripathy, S. Mechanism of enhanced light output efficiency in InGaN-based microlight emitting diodes. *J. Appl. Phys.* **2003**, *93*, 5978–5982. [[CrossRef](#)]
18. Wang, Y.; Wang, Y.; Chi, N.; Yu, J.; Shang, H. Demonstration of 575-Mb/s downlink and 225-Mb/s uplink bi-directional SCM-WDM visible light communication using RGB LED and phosphor-based LED. *Opt. Express* **2013**, *21*, 1203–1208. [[CrossRef](#)] [[PubMed](#)]
19. Lin, W.-Y.; Chen, C.-Y.; Lu, H.-H.; Chang, C.-H.; Lin, Y.-P.; Lin, H.-C.; Wu, H.-W. 10m/500Mbps WDM visible light communication systems. *Opt. Express* **2012**, *20*, 9919–9924. [[CrossRef](#)] [[PubMed](#)]
20. Watson, S.; Tan, M.; Najda, S.P.; Perlin, P.; Leszczynski, M.; Targowski, G.; Grzanka, S.; Kelly, A.E. Visible light communications using a directly modulated 422 nm GaN laser diode. *Opt. Lett.* **2013**, *38*, 3792–3794. [[CrossRef](#)] [[PubMed](#)]
21. Chen, C.-Y.; Wu, P.-Y.; Lu, H.-H.; Lin, Y.-P.; Wen, J.-Y.; Hu, F.-C. Bidirectional 16-QAM OFDM in-building network over SMF and free-space VLC transport. *Opt. Lett.* **2013**, *38*, 2345–2347. [[CrossRef](#)] [[PubMed](#)]
22. Chi, Y.-C.; Hsieh, D.-H.; Tsai, C.-T.; Chen, H.-Y.; Kuo, H.-C.; Lin, G.-R. 450-nm GaN laser diode enables high-speed visible light communication with 9-Gbps QAM-OFDM. *Opt. Express* **2015**, *23*, 13051–13059. [[CrossRef](#)]
23. Lee, C.; Shen, C.; Oubei, H.M.; Cantore, M.; Janjua, B.; Ng, T.K.; Farrell, R.M.; El-Desouki, M.M.; Speck, J.S.; Nakamura, S.; et al. 2 Gbit/s data transmission from an unfiltered laser-based phosphor-converted white lighting communication system. *Opt. Express* **2015**, *23*, 29779–29787. [[CrossRef](#)] [[PubMed](#)]
24. Retamal, J.R.D.; Oubei, H.M.; Janjua, B.; Chi, Y.-C.; Wang, H.-Y.; Tsai, C.-T.; Ng, T.K.; Hsieh, D.-H.; Kuo, H.-C.; Alouini, M.-S.; et al. 4-Gbit/s visible light communication link based on 16-QAM OFDM transmission over remote phosphor-film converted white light by using blue laser diode. *Opt. Express* **2015**, *23*, 33656–33666. [[CrossRef](#)] [[PubMed](#)]
25. Chi, Y.-C.; Hsieh, D.-H.; Lin, C.-Y.; Chen, H.-Y.; Huang, C.-Y.; He, J.-H.; Ooi, B.; DenBaars, S.P.; Nakamura, S.; Kuo, H.-C.; et al. Phosphorous Diffuser Diverged Blue Laser Diode for Indoor Lighting and Communication. *Sci. Rep.* **2015**, *5*, 18690. [[CrossRef](#)]
26. Tsonev, D.; Videv, S.; Haas, H. Towards a 100 Gb/s visible light wireless access network. *Opt. Express* **2015**, *23*, 1627–1637. [[CrossRef](#)]
27. Wu, T.-C.; Chi, Y.-C.; Wang, H.-Y.; Tsai, C.-T.; Huang, Y.-F.; Lin, G.-R. Tricolor R/G/B Laser Diode Based Eye-Safe White Lighting Communication Beyond 8 Gbit/s. *Sci. Rep.* **2017**, *7*, 11. [[CrossRef](#)]
28. Tsai, C.-T.; Cheng, C.-H.; Kuo, H.-C.; Lin, G.-R. Toward high-speed visible laser lighting based optical wireless communications. *Prog. Quantum Electron.* **2019**, *67*, 100225. [[CrossRef](#)]
29. Lin, C.C.; Liu, R.-S. Advances in Phosphors for Light-emitting Diodes. *J. Phys. Chem. Lett.* **2011**, *2*, 1268–1277. [[CrossRef](#)] [[PubMed](#)]
30. Deng, P.; Kavehrad, M. Effect of white LED DC-bias on modulation speed for visible light communications. *arXiv* **2016**, arXiv:1612.08477.
31. Zhu, S.; Lin, S.; Li, J.; Yu, Z.; Cao, H.; Yang, C.; Li, J.; Zhao, L. Influence of quantum confined Stark effect and carrier localization effect on modulation bandwidth for GaN-based LEDs. *Appl. Phys. Lett.* **2017**, *111*, 171105. [[CrossRef](#)]
32. Ryou, J.-H.; Lee, W.; Limb, J.; Yoo, D.; Liu, J.P.; Dupuis, R.D.; Wu, Z.H.; Fischer, A.M.; Ponce, F.A. Control of quantum-confined Stark effect in InGaN/GaN multiple quantum well active region by p-type layer for III-nitride-based visible light emitting diodes. *Appl. Phys. Lett.* **2008**, *92*, 101113. [[CrossRef](#)]
33. Zhang, Y.; Smith, R.M.; Hou, Y.; Xu, B.; Gong, Y.; Bai, J.; Wang, T. Stokes shift in semi-polar (112–2) InGaN/GaN multiple quantum wells. *Appl. Phys. Lett.* **2016**, *108*, 031108. [[CrossRef](#)]
34. Piprek, J. Efficiency droop in nitride-based light-emitting diodes. *Physica Status Solidi A* **2010**, *207*, 2217–2225. [[CrossRef](#)]
35. Kozłowski, G.; Schulz, S.; Corbett, B. Polarization matching design of InGaN-based semi-polar quantum wells—A case study of (112–2) orientation. *Appl. Phys. Lett.* **2014**, *104*, 051128. [[CrossRef](#)]
36. Chen, S.-W.H.; Huang, Y.-M.; Singh, K.J.; Hsu, Y.-C.; Liou, F.-J.; Song, J.; Choi, J.; Lee, P.-T.; Lin, C.-C.; Chen, Z.; et al. Full-color micro-LED display with high color stability using semipolar (20–21) InGaN LEDs and quantum-dot photoresist. *Photon. Res.* **2020**, *8*, 630–636. [[CrossRef](#)]
37. Rosales, D.; Gil, B.; Bretagnon, T.; Guizal, B.; Izyumskaya, N.; Monavarian, M.; Zhang, F.; Okur, S.; Avrutin, V.; Özgür, Ü.; et al. Recombination dynamics of excitons with low non-radiative component in semi-polar (10-11)-oriented GaN/AlGaIn multiple quantum wells. *J. Appl. Phys.* **2014**, *116*, 093517. [[CrossRef](#)]
38. Zhou, X.; Tian, P.; Sher, C.-W.; Wu, J.; Liu, H.; Liu, R.; Kuo, H.-C. Growth, transfer printing and colour conversion techniques towards full-colour micro-LED display. *Prog. Quantum Electron.* **2020**, *71*, 100263. [[CrossRef](#)]
39. Liu, Z.; Lin, C.-H.; Hyun, B.-R.; Sher, C.-W.; Lv, Z.; Luo, B.; Jiang, F.; Wu, T.; Ho, C.-H.; Kuo, H.-C.; et al. Micro-light-emitting diodes with quantum dots in display technology. *Light Sci. Appl.* **2020**, *9*, 83. [[CrossRef](#)]
40. Okur, S.; Nami, M.; Rishinaramangalam, A.K.; Oh, S.H.; DenBaars, S.P.; Liu, S.; Brener, I.; Feezell, D.F. Internal quantum efficiency and carrier dynamics in semipolar (20-2-1) InGaN/GaN light-emitting diodes. *Opt. Express* **2017**, *25*, 2178–2186. [[CrossRef](#)]
41. Liao, C.; Chang, Y.; Ho, C.; Wu, M. High-Speed GaN-Based Blue Light-Emitting Diodes with Gallium-Doped ZnO Current Spreading Layer. *IEEE Electron. Device Lett.* **2013**, *34*, 611–613. [[CrossRef](#)]

42. Liao, C.; Ho, C.; Chang, Y.; Wu, C.; Wu, M. High-Speed Light-Emitting Diodes Emitting at 500 nm with 463-MHz Modulation Bandwidth. *IEEE Electron. Device Lett.* **2014**, *35*, 563–565. [[CrossRef](#)]
43. McKendry, J.J.D.; Massoubre, D.; Zhang, S.; Rae, B.R.; Green, R.P.; Gu, E.; Henderson, R.K.; Kelly, A.E.; Dawson, M.D. Visible-Light Communications Using a CMOS-Controlled Micro-Light-Emitting-Diode Array. *J. Lightwave Technol.* **2012**, *30*, 61–67. [[CrossRef](#)]
44. Wun, J.; Lin, C.; Chen, W.; Sheu, J.; Lin, C.; Li, Y.; Bowers, J.E.; Shi, J.; Vinogradov, J.; Kruglov, R.; et al. GaN-Based Miniaturized Cyan Light-Emitting Diodes on a Patterned Sapphire Substrate with Improved Fiber Coupling for Very High-Speed Plastic Optical Fiber Communication. *IEEE Photonics J.* **2012**, *4*, 1520–1529. [[CrossRef](#)]
45. Shi, J.; Chi, K.; Wun, J.; Bowers, J.E.; Shih, Y.; Sheu, J. III-Nitride-Based Cyan Light-Emitting Diodes with GHz Bandwidth for High-Speed Visible Light Communication. *IEEE Electron. Device Lett.* **2016**, *37*, 894–897. [[CrossRef](#)]
46. Monavarian, M.; Rashidi, A.; Aragon, A.A.; Nami, M.; Oh, S.H.; DenBaars, S.P.; Feezell, D. Trade-off between bandwidth and efficiency in semipolar (20°–1°) InGaN/GaN single- and multiple-quantum-well light-emitting diodes. *Appl. Phys. Lett.* **2018**, *112*, 191102. [[CrossRef](#)]
47. Lefebvre, P.; Allègre, J.; Mathieu, H. Recombination dynamics of excitons in III-nitride layers and quantum wells. *Mater. Sci. Eng. B* **1999**, *59*, 307–314. [[CrossRef](#)]
48. Malinauskas, T.; Miasojedovas, S.; Aleksiejūnas, R.; Juršėnas, S.; Jarašiūnas, K.; Nomura, M.; Arakawa, Y.; Shimura, T.; Kuroda, K. Direct study of nonlinear carrier recombination in InGaN quantum well structures. *Physica Status Solidi C* **2011**, *8*, 2381–2383. [[CrossRef](#)]
49. Mickevičius, J.; Tamulaitis, G.; Kuokštis, E.; Liu, K.; Shur, M.S.; Zhang, J.P.; Gaska, R. Well-width-dependent carrier lifetime in AlGaIn/AlGaIn quantum wells. *Appl. Phys. Lett.* **2007**, *90*, 131907. [[CrossRef](#)]
50. Huang, S.; Xian, Y.; Fan, B.; Zheng, Z.; Chen, Z.; Jia, W.; Jiang, H.; Wang, G. Contrary luminescence behaviors of InGaIn/GaN light emitting diodes caused by carrier tunneling leakage. *J. Appl. Phys.* **2011**, *110*, 064511. [[CrossRef](#)]
51. Li, Y.-L.; Huang, Y.-R.; Lai, Y.-H. Efficiency droop behaviors of InGaIn/GaN multiple-quantum-well light-emitting diodes with varying quantum well thickness. *Appl. Phys. Lett.* **2007**, *91*, 181113. [[CrossRef](#)]
52. James Singh, K.; Huang, Y.-M.; Ahmed, T.; Liu, A.-C.; Huang Chen, S.-W.; Liou, F.-J.; Wu, T.; Lin, C.-C.; Chow, C.-W.; Lin, G.-R.; et al. Micro-LED as a Promising Candidate for High-Speed Visible Light Communication. *Appl. Sci.* **2020**, *10*, 7384. [[CrossRef](#)]
53. Choi, H.W.; Liu, C.; Gu, E.; McConnell, G.; Girkin, J.M.; Watson, I.M.; Dawson, M.D. GaN micro-light-emitting diode arrays with monolithically integrated sapphire microlenses. *Appl. Phys. Lett.* **2004**, *84*, 2253–2255. [[CrossRef](#)]
54. Lin, H.-Y.; Sher, C.-W.; Hsieh, D.-H.; Chen, X.-Y.; Chen, H.-M.P.; Chen, T.-M.; Lau, K.-M.; Chen, C.-H.; Lin, C.-C.; Kuo, H.-C. Optical cross-talk reduction in a quantum-dot-based full-color micro-light-emitting-diode display by a lithographic-fabricated photoresist mold. *Photon. Res.* **2017**, *5*, 411–416. [[CrossRef](#)]
55. Shi, J.; Sheu, J.; Chen, C.; Lin, G.; Lai, W. High-Speed GaN-Based Green Light-Emitting Diodes with Partially n-Doped Active Layers and Current-Confined Apertures. *IEEE Electron. Device Lett.* **2008**, *29*, 158–160. [[CrossRef](#)]
56. Kelly, A.E.; McKendry, J.J.D.; Zhang, S.; Massoubre, D.; Rae, B.R.; Green, R.P.; Henderson, R.K.; Dawson, M.D. High-speed GaN micro-LED arrays for data communications. In Proceedings of the 2012 14th International Conference on Transparent Optical Networks (ICTON), Coventry, UK, 2–5 July 2012; pp. 1–5.
57. Corbett, B.; Quan, Z.; Dinh, D.V.; Kozłowski, G.; O'Mahony, D.; Akhter, M.; Schulz, S.; Parbrook, P.; Maaskant, P.; Caliebe, M.; et al. *Development of Semipolar (11–22) LEDs on GaN Templates*; SPIE: Bellingham, DC, USA, 2016; Volume 9768.
58. Li, J.; Gou, P.; Chi, N.; Ou, H. Enhanced Emission and Modulation Properties of Localized Surface Plasma Coupled GaN-based Green Light-Emitting Diodes. In Proceedings of the Optical Fiber Communication Conference, San Diego, CA, USA, 11 March 2018. paper Th2A.65.
59. Rashidi, A.; Monavarian, M.; Aragon, A.; Rishinaramangalam, A.; Feezell, D. Nonpolar m-Plane InGaIn/GaN Micro-Scale Light-Emitting Diode With 1.5 GHz Modulation Bandwidth. *IEEE Electron. Device Lett.* **2018**, *39*, 520–523. [[CrossRef](#)]
60. Khoury, M.; Li, H.; Li, P.; Chow, Y.C.; Bonef, B.; Zhang, H.; Wong, M.S.; Pinna, S.; Song, J.; Choi, J.; et al. Polarized monolithic white semipolar (20–21) InGaIn light-emitting diodes grown on high quality (20–21) GaN/sapphire templates and its application to visible light communication. *Nano Energy* **2020**, *67*, 104236. [[CrossRef](#)]
61. Chen, S.-W.H.; Huang, Y.-M.; Chang, Y.-H.; Lin, Y.; Liou, F.-J.; Hsu, Y.-C.; Song, J.; Choi, J.; Chow, C.-W.; Lin, C.-C.; et al. High-Bandwidth Green Semipolar (20–21) InGaIn/GaN Micro Light-Emitting Diodes for Visible Light Communication. *ACS Photonics* **2020**, *7*, 2228–2235. [[CrossRef](#)]
62. Hagggar, J.I.H.; Cai, Y.; Ghataora, S.S.; Smith, R.M.; Bai, J.; Wang, T. High Modulation Bandwidth of Semipolar (11–22) InGaIn/GaN LEDs with Long Wavelength Emission. *ACS Appl. Electron. Mater.* **2020**, *2*, 2363–2368. [[CrossRef](#)]
63. Liu, X.; Wei, Z.; Li, M.; Wang, L.; Liu, Z.; Yu, C.; Wang, L.; Luo, Y.; Fu, H.Y. Experimental investigation of 16.6 Gbps SDM-WDM visible light communication based on a neural network receiver and tricolor mini-LEDs. *Opt. Lett.* **2021**, *46*, 2888–2891. [[CrossRef](#)]
64. Wang, L.; Wang, L.; Chen, C.-J.; Chen, K.-C.; Hao, Z.; Luo, Y.; Sun, C.; Wu, M.-C.; Yu, J.; Han, Y.; et al. Green InGaIn Quantum Dots Breaking through Efficiency and Bandwidth Bottlenecks of Micro-LEDs. *Laser Photonics Rev.* **2021**, *15*, 2000406. [[CrossRef](#)]
65. Shen, C. Visible Lasers and Emerging Color Converters for Lighting and Visible Light Communications. In Proceedings of the Light, Energy and the Environment, Boulder, CO, USA, 6 November 2017. paper SW3C.2.
66. Nakamura, S.; Chichibu, S.F. *Introduction to Nitride Semiconductor Blue Lasers and Light Emitting Diodes*; CRC Press: Boca Raton, FL, USA, 2000.

67. Shamim, M.H.M.; Shemis, M.A.; Shen, C.; Oubei, H.M.; Ng, T.K.; Ooi, B.S.; Khan, M.Z.M. Investigation of Self-Injection Locked Visible Laser Diodes for High Bit-Rate Visible Light Communication. *IEEE Photonics J.* **2018**, *10*, 7905611. [[CrossRef](#)]
68. Mukhtar, S.; Xiaobin, S.; Ashry, I.; Ng, T.K.; Ooi, B.S.; Khan, M.Z.M. Tunable Violet Laser Diode System for Optical Wireless Communication. *IEEE Photonics Technol. Lett.* **2020**, *32*, 546–549. [[CrossRef](#)]
69. Holguin-Lerma, J.A.; Kong, M.; Alkhazragi, O.; Sun, X.; Khee Ng, T.; Ooi, B.S. 480-nm distributed-feedback InGaN laser diode for 10.5-Gbit/s visible-light communication. *Opt. Lett.* **2020**, *45*, 742–745. [[CrossRef](#)] [[PubMed](#)]
70. Denault, K.A.; Cantore, M.; Nakamura, S.; DenBaars, S.P.; Seshadri, R. Efficient and stable laser-driven white lighting. *AIP Adv.* **2013**, *3*, 072107. [[CrossRef](#)]
71. Tsao, J.Y.; Crawford, M.H.; Coltrin, M.E.; Fischer, A.J.; Koleske, D.D.; Subramania, G.S.; Wang, G.T.; Wierer, J.J.; Karlicek Jr., R. F. Toward Smart and Ultra-efficient Solid-State Lighting. *Adv. Opt. Mater.* **2014**, *2*, 809–836. [[CrossRef](#)]
72. SLD Laser Technology and Applications. Available online: <https://www.displaydaily.com/article/display-daily/sld-laser-technology-and-applications> (accessed on 20 July 2021).
73. Lee, C.; Islim, M.S.; Videv, S.; Sparks, A.; Shah, B.; Rudy, P.; McLaurin, M.; Haas, H.; Raring, J. *Advanced LiFi Technology: Laser Light*; SPIE: Bellingham, DC, USA, 2020; Volume 11302.
74. Rossetti, M.; Napierala, J.; Matuschek, N.; Achatz, U.; Duelk, M.; Vélez, C.; Castiglia, A.; Grandjean, N.; Dorsaz, J.; Feltin, E. *Superluminescent Light Emitting Diodes: The Best out of Two Worlds*; SPIE: Bellingham, DC, USA, 2012; Volume 8252.
75. Hu, F.; Holguin-Lerma, J.; Mao, Y.; Shen, C.; Sun, X.; Kong, M.; Ng, T.K.; Ooi, B.; Chi, N. *3.8-Gbit/s Visible Light Communication (VLCa) Based on 443-nm Superluminescent Diode and Bit-Loading Discrete-Multiple-Tone (DMT) Modulation Scheme*; SPIE: Bellingham, DC, USA, 2020; Volume 11307.
76. Kopp, F.; Eichler, C.; Lell, A.; Tautz, S.; Ristić, J.; Stojetz, B.; Höß, C.; Weig, T.; Schwarz, U.T.; Strauss, U. Blue superluminescent light-emitting diodes with output power above 100 mW for picoprojection. *Jpn. J. Appl. Phys.* **2013**, *52*, 08JH07. [[CrossRef](#)]
77. Shen, C.; Ng, T.K.; Leonard, J.T.; Pourhashemi, A.; Nakamura, S.; DenBaars, S.P.; Speck, J.S.; Alyamani, A.Y.; El-desouki, M.M.; Ooi, B.S. High-brightness semipolar (20 $\bar{2}1$) blue InGaN/GaN superluminescent diodes for droop-free solid-state lighting and visible-light communications. *Opt. Lett.* **2016**, *41*, 2608–2611. [[CrossRef](#)] [[PubMed](#)]
78. Shen, C.; Leonard, J.T.; Young, E.C.; Ng, T.K.; DenBaars, S.P.; Speck, J.S.; Nakamura, S.; Alyamani, A.Y.; El-Desouki, M.M.; Ooi, B.S. GHz modulation bandwidth from single-longitudinal mode violet-blue VCSEL using nonpolar InGaN/GaN QWs. In Proceedings of the 2016 Conference on Lasers and Electro-Optics (CLEO), San Jose, CA, USA, 2016, 5–10 June 2016; pp. 1–2.
79. Sarzała, R.P.; Śpiewak, P.; Nakwaski, W.; Wasiak, M. Cavity designs for nitride VCSELs with dielectric DBRs operating efficiently at different temperatures. *Opt. Laser Technol.* **2020**, *132*, 106482. [[CrossRef](#)]
80. Hsu, C.; Chow, C.; Lu, I.; Liu, Y.; Yeh, C.; Liu, Y. High Speed Imaging 3 × 3 MIMO Phosphor White-Light LED Based Visible Light Communication System. *IEEE Photonics J.* **2016**, *8*, 7907406. [[CrossRef](#)]
81. Cossu, G.; Khalid, A.M.; Choudhury, P.; Corsini, R.; Ciaramella, E. 3.4 Gbit/s visible optical wireless transmission based on RGB LED. *Opt. Express* **2012**, *20*, B501–B506. [[CrossRef](#)]
82. Lu, I.C.; Lai, C.-H.; Yeh, C.-H.; Chen, J. 6.36 Gbit/s RGB LED-based WDM MIMO Visible Light Communication System Employing OFDM Modulation. In Proceedings of the Optical Fiber Communication Conference, Los Angeles, CA, USA, 19 March 2017; paper W2A.39.
83. Chi, N.; Zhang, M.; Zhou, Y.; Zhao, J. 3.375-Gb/s RGB-LED based WDM visible light communication system employing PAM-8 modulation with phase shifted Manchester coding. *Opt. Express* **2016**, *24*, 21663–21673. [[CrossRef](#)]
84. Zhu, X.; Wang, F.; Shi, M.; Chi, N.; Liu, J.; Jiang, F. 10.72Gb/s Visible Light Communication System Based on Single Packaged RGB-LED Utilizing QAM-DMT Modulation with Hardware Pre-Equalization. In Proceedings of the Optical Fiber Communication Conference, San Diego, CA, USA, 11 March 2018. paper M3K.3.
85. Tsonev, D.; Chun, H.; Rajbhandari, S.; McKendry, J.J.D.; Videv, S.; Gu, E.; Haji, M.; Watson, S.; Kelly, A.E.; Faulkner, G.; et al. A 3-Gb/s Single-LED OFDM-Based Wireless VLC Link Using a Gallium Nitride μ LED. *IEEE Photonics Technol. Lett.* **2014**, *26*, 637–640. [[CrossRef](#)]
86. Islim, M.S.; Ferreira, R.X.; He, X.; Xie, E.; Videv, S.; Viola, S.; Watson, S.; Bamiedakis, N.; Penty, R.V.; White, I.H.; et al. Towards 10 Gb/s orthogonal frequency division multiplexing-based visible light communication using a GaN violet micro-LED. *Photon. Res.* **2017**, *5*, A35–A43. [[CrossRef](#)]
87. He, X.; Xie, E.; Islim, M.S.; Purwita, A.A.; McKendry, J.J.D.; Gu, E.; Haas, H.; Dawson, M.D. 1 Gbps free-space deep-ultraviolet communications based on III-nitride micro-LEDs emitting at 262 nm. *Photon. Res.* **2019**, *7*, B41–B47. [[CrossRef](#)]
88. Chang, C.-H.; Li, C.-Y.; Lu, H.-H.; Lin, C.-Y.; Chen, J.-H.; Wan, Z.-W.; Cheng, C.-J. A 100-Gb/s Multiple-Input Multiple-Output Visible Laser Light Communication System. *J. Lightwave Technol.* **2014**, *32*, 4121–4127. [[CrossRef](#)]
89. Lee, C.; Zhang, C.; Cantore, M.; Farrell, R.M.; Oh, S.H.; Margalith, T.; Speck, J.S.; Nakamura, S.; Bowers, J.E.; DenBaars, S.P. 4 Gbps direct modulation of 450 nm GaN laser for high-speed visible light communication. *Opt. Express* **2015**, *23*, 16232–16237. [[CrossRef](#)] [[PubMed](#)]
90. Huang, Y.-F.; Chi, Y.-C.; Kao, H.-Y.; Tsai, C.-T.; Wang, H.-Y.; Kuo, H.-C.; Nakamura, S.; Huang, D.-W.; Lin, G.-R. Blue Laser Diode Based Free-space Optical Data Transmission elevated to 18 Gbps over 16 m. *Sci. Rep.* **2017**, *7*, 10478. [[CrossRef](#)] [[PubMed](#)]
91. Wang, W.-C.; Wang, H.-Y.; Lin, G.-R. Ultrahigh-speed violet laser diode based free-space optical communication beyond 25 Gbit/s. *Sci. Rep.* **2018**, *8*, 13142. [[CrossRef](#)]

92. Lu, I.; Yeh, C.; Hsu, D.; Chow, C. Utilization of 1-GHz VCSEL for 11.1-Gbps OFDM VLC Wireless Communication. *IEEE Photonics J.* **2016**, *8*, 7904106. [[CrossRef](#)]
93. Yeh, C.-H.; Wei, L.-Y.; Chow, C.-W. Using a Single VCSEL Source Employing OFDM Downstream Signal and Remodulated OOK Upstream Signal for Bi-directional Visible Light Communications. *Sci. Rep.* **2017**, *7*, 15846. [[CrossRef](#)] [[PubMed](#)]
94. Wei, L.; Chow, C.; Hsu, C.; Yeh, C. Bidirectional Visible Light Communication System Using a Single VCSEL With Predistortion to Enhance the Upstream Remodulation. *IEEE Photonics J.* **2018**, *10*, 7903407. [[CrossRef](#)]
95. Yeh, C.; Chow, C.; Wei, L. 1250 Mbit/s OOK Wireless White-Light VLC Transmission Based on Phosphor Laser Diode. *IEEE Photonics J.* **2019**, *11*, 7903205. [[CrossRef](#)]
96. Lee, C.; Shen, C.; Cozzan, C.; Farrell, R.M.; Speck, J.S.; Nakamura, S.; Ooi, B.S.; DenBaars, S.P. Gigabit-per-second white light-based visible light communication using near-ultraviolet laser diode and red-, green-, and blue-emitting phosphors. *Opt. Express* **2017**, *25*, 17480–17487. [[CrossRef](#)]
97. Wei, L.-Y.; Chow, C.-W.; Liu, Y.; Yeh, C.-H. Multi-Gbit/s phosphor-based white-light and blue-filter-free visible light communication and lighting system with practical transmission distance. *Opt. Express* **2020**, *28*, 7375–7381. [[CrossRef](#)]
98. Wei, L.-Y.; Liu, Y.; Chow, C.-W.; Chen, G.-H.; Peng, C.-W.; Guo, P.-C.; Tsai, J.-F.; Yeh, C.-H. 6.915-Gbit/s white-light phosphor laser diode-based DCO-OFDM visible light communication (VLC) system with functional transmission distance. *Electron. Lett.* **2020**, *56*, 945–947. [[CrossRef](#)]
99. Wei, L.-Y.; Hsu, C.-W.; Chow, C.-W.; Yeh, C.-H. 20.231 Gbit/s tricolor red/green/blue laser diode based bidirectional signal remodulation visible-light communication system. *Photon. Res.* **2018**, *6*, 422–426. [[CrossRef](#)]
100. Chow, C.W.; Chang, Y.H.; Wei, L.Y.; Yeh, C.H.; Liu, Y. 26.228-Gbit/s RGBV Visible Light Communication (VLC) with 2-m Free Space Transmission. In Proceedings of the 2020 Opto-Electronics and Communications Conference (OECC), Taipei, Taiwan, 4–8 October 2020; pp. 1–3.
101. Sze, S.M.; Li, Y.; Ng, K.K. *Physics of Semiconductor Devices*; John Wiley & Sons: Hoboken, NJ, USA, 2021.
102. Prasad, S.; Schumacher, H.; Gopinath, A. *High-Speed Electronics and Optoelectronics: Devices and Circuits*; Cambridge University Press: Cambridge, UK, 2009.
103. Ang, K.-W.; Ng, J.W.; Lo, G.-Q.; Kwong, D.-L. Impact of field-enhanced band-traps-band tunneling on the dark current generation in germanium p-i-n photodetector. *Appl. Phys. Lett.* **2009**, *94*, 223515. [[CrossRef](#)]
104. Takenaka, M.; Morii, K.; Sugiyama, M.; Nakano, Y.; Takagi, S. Dark current reduction of Ge photodetector by GeO₂ surface passivation and gas-phase doping. *Opt. Express* **2012**, *20*, 8718–8725. [[CrossRef](#)] [[PubMed](#)]
105. Yan, D.; Mao, X.; Cong, J.; Xie, S. Fully integrated receiver for free-space visible light communication. *IEICE Electron. Express* **2019**, *16*, 20190418. [[CrossRef](#)]
106. Mica, N.A.; Bian, R.; Manousiadis, P.; Jagadamma, L.K.; Tavakkolnia, I.; Haas, H.; Turnbull, G.A.; Samuel, I.D.W. Triple-cation perovskite solar cells for visible light communications. *Photon. Res.* **2020**, *8*, A16–A24. [[CrossRef](#)]
107. Kang, C.H.; Liu, G.; Lee, C.; Alkhazragi, O.; Wagstaff, J.M.; Li, K.-H.; Alhawaj, F.; Ng, T.K.; Speck, J.S.; Nakamura, S. Semipolar (20-2-1) InGa_N/Ga_N micro-photodetector for gigabit-per-second visible light communication. *Appl. Phys. Express* **2019**, *13*, 014001. [[CrossRef](#)]
108. Zhang, T.; Wu, J.; Zhang, P.; Ahmad, W.; Wang, Y.; Alqahtani, M.; Chen, H.; Gao, C.; Chen, Z.D.; Wang, Z.; et al. High Speed and Stable Solution-Processed Triple Cation Perovskite Photodetectors. *Adv. Opt. Mater.* **2018**, *6*, 1701341. [[CrossRef](#)]
109. Kang, C.H.; Trichili, A.; Alkhazragi, O.; Zhang, H.; Subedi, R.C.; Guo, Y.; Mitra, S.; Shen, C.; Roqan, I.S.; Ng, T.K.; et al. Ultraviolet-to-blue color-converting scintillating-fibers photoreceiver for 375-nm laser-based underwater wireless optical communication. *Opt. Express* **2019**, *27*, 30450–30461. [[CrossRef](#)] [[PubMed](#)]
110. Kosman, J.; Almer, O.; Abbas, T.A.; Dutton, N.; Walker, R.; Videv, S.; Moore, K.; Haas, H.; Henderson, R. A 500Mb/s -46.1dBm CMOS SPAD Receiver for Laser Diode Visible-Light Communications. In Proceedings of the 2019 IEEE International Solid-State Circuits Conference—(ISSCC), San Francisco, CA, USA, 17–21 February 2019; pp. 468–470.
111. Alkhazragi, O.; Kang, C.H.; Kong, M.; Liu, G.; Lee, C.; Li, K.; Zhang, H.; Wagstaff, J.M.; Alhawaj, F.; Ng, T.K.; et al. 7.4-Gbit/s Visible-Light Communication Utilizing Wavelength-Selective Semipolar Micro-Photodetector. *IEEE Photonics Technol. Lett.* **2020**, *32*, 767–770. [[CrossRef](#)]
112. Huang, S.; Wu, Q.; Jia, Z.; Jin, X.; Fu, X.; Huang, H.; Zhang, X.; Yao, J.; Xu, J. Black Silicon Photodetector with Excellent Comprehensive Properties by Rapid Thermal Annealing and Hydrogenated Surface Passivation. *Adv. Opt. Mater.* **2020**, *8*, 1901808. [[CrossRef](#)]
113. Milovančev, D.; Jukić, T.; Vokić, N.; Brandl, P.; Steindl, B.; Zimmermann, H. VLC Using 800- μ m Diameter APD Receiver Integrated in Standard 0.35- μ m BiCMOS Technology. *IEEE Photonics J.* **2021**, *13*, 7900513. [[CrossRef](#)]
114. Pathak, P.H.; Feng, X.; Hu, P.; Mohapatra, P. Visible Light Communication, Networking, and Sensing: A Survey, Potential and Challenges. *IEEE Commun. Surv. Tutor.* **2015**, *17*, 2047–2077. [[CrossRef](#)]
115. Berman, S.M.; Greenhouse, D.S.; Bailey, I.L.; Clear, R.D.; Raasch, T.W. Human electroretinogram responses to video displays, fluorescent lighting, and other high frequency sources. *Optom. Vis. Sci.* **1991**, *68*, 645–662. [[CrossRef](#)]
116. Hranilovic, S.; Kschischang, F.R. Short-range wireless optical communication using pixilated transmitters and imaging receivers. In Proceedings of the 2004 IEEE International Conference on Communications (IEEE Cat. No.04CH37577), Paris, France, 20–24 June 2004; Volume 892, pp. 891–895.

117. Elganimi, T.Y. Performance comparison between OOK, PPM and pam modulation schemes for free space optical (FSO) communication systems: Analytical study. *Int. J. Comput. Appl.* **2013**, *79*, 11.
118. Elganimi, T.Y. Studying the BER performance, power- and bandwidth- efficiency for FSO communication systems under various modulation schemes. In Proceedings of the 2013 IEEE Jordan Conference on Applied Electrical Engineering and Computing Technologies (AEECT), Amman, Jordan, 3–5 December 2013; pp. 1–6.
119. Binh, L.N. *Advanced Digital: Optical Communications*; CRC Press: Boca Raton, FL, USA, 2015.
120. Lathi, B.P. *Modern Digital and Analog Communication Systems*; Oxford University Press, Inc.: Oxford, UK, 1995.
121. Xiong, F. *Digital Modulation Techniques*, 2nd ed.; Artech House, Inc.: Boston, MA, USA, 2006.
122. Dimitrov, S.; Sinanovic, S.; Haas, H. Signal Shaping and Modulation for Optical Wireless Communication. *J. Lightwave Technol.* **2012**, *30*, 1319–1328. [[CrossRef](#)]
123. IEEE Approved Draft Standard for Short-Range Wireless Optical Communication Using Visible Light. Available online: <https://ieeexplore.ieee.org/servlet/opac?punumber=6016193> (accessed on 23 July 2021).
124. Singh, R.; O'Farrell, T.; David, J.P.R. An Enhanced Color Shift Keying Modulation Scheme for High-Speed Wireless Visible Light Communications. *J. Lightwave Technol.* **2014**, *32*, 2582–2592. [[CrossRef](#)]
125. Dimitrakopoulos, G.; Demestichas, P. Intelligent transportation systems. *IEEE Veh. Technol. Mag.* **2010**, *5*, 77–84. [[CrossRef](#)]
126. Do, T.-H.; Yoo, M. An in-Depth Survey of Visible Light Communication Based Positioning Systems. *Sensors* **2016**, *16*, 678. [[CrossRef](#)]
127. Căilean, A.; Dimian, M. Current Challenges for Visible Light Communications Usage in Vehicle Applications: A Survey. *IEEE Commun. Surv. Tutor.* **2017**, *19*, 2681–2703. [[CrossRef](#)]
128. Kaushal, H.; Kaddoum, G. Underwater Optical Wireless Communication. *IEEE Access* **2016**, *4*, 1518–1547. [[CrossRef](#)]
129. Wang, Y.; Chi, N.; Wang, Y.; Tao, L.; Shi, J. Network Architecture of a High-Speed Visible Light Communication Local Area Network. *IEEE Photonics Technol. Lett.* **2015**, *27*, 197–200. [[CrossRef](#)]
130. Curcio, J.A.; Petty, C.C. The Near Infrared Absorption Spectrum of Liquid Water. *J. Opt. Soc. Am.* **1951**, *41*, 302–304. [[CrossRef](#)]
131. Lin, R.; Liu, X.; Zhou, G.; Qian, Z.; Cui, X.; Tian, P. InGaN Micro-LED Array Enabled Advanced Underwater Wireless Optical Communication and Underwater Charging. *Adv. Opt. Mater.* **2021**, *9*, 2002211. [[CrossRef](#)]
132. Prieur, L.; Sathyendranath, S. An optical classification of coastal and oceanic waters based on the specific spectral absorption curves of phytoplankton pigments, dissolved organic matter, and other particulate materials. *Limnol. Oceanogr.* **1981**, *26*, 671–689. [[CrossRef](#)]
133. Li, C.; Lu, H.; Tsai, W.; Wang, Z.; Hung, C.; Su, C.; Lu, Y. A 5 m/25 Gbps Underwater Wireless Optical Communication System. *IEEE Photonics J.* **2018**, *10*, 7904909. [[CrossRef](#)]
134. Wu, T.; Yue, L.; Huang, Y.-M.; Liu, M.; James Singh, K.; Lin, W.; Lu, T.; Heng, X.; Zhou, Z.; Kuo, H.-C.; et al. A highly stable full-color display device with VLC application potential using semipolar micro-LEDs and all-inorganic encapsulated perovskite nanocrystal. *Photon. Res.* **2021**. [[CrossRef](#)]
135. Liu, X.; Lin, R.; Chen, H.; Zhang, S.; Qian, Z.; Zhou, G.; Chen, X.; Zhou, X.; Zheng, L.; Liu, R.; et al. High-Bandwidth InGaN Self-Powered Detector Arrays toward MIMO Visible Light Communication Based on Micro-LED Arrays. *ACS Photonics* **2019**, *6*, 3186–3195. [[CrossRef](#)]
136. Chi, N.; Zhou, Y.; Wei, Y.; Hu, F. Visible Light Communication in 6G: Advances, Challenges, and Prospects. *IEEE Veh. Technol. Mag.* **2020**, *15*, 93–102. [[CrossRef](#)]
137. Lin, G.-R.; Kuo, H.-C.; Cheng, C.-H.; Wu, Y.-C.; Huang, Y.; Liou, F.-J.; Lee, Y.-C. Ultrafast 2 × 2 Green Micro-LED Array for Optical Wireless Communication beyond 5 Gbit/s. *Photon. Res.* **2021**. [[CrossRef](#)]
138. Guo, X.; Chi, N. Superposed 32QAM Constellation Design for 2 × 2 Spatial Multiplexing MIMO VLC Systems. *J. Lightwave Technol.* **2020**, *38*, 1702–1711. [[CrossRef](#)]
139. Sabouri, S.; Jamshidi, K. Design Considerations of Silicon Nitride Optical Phased Array for Visible Light Communications. *IEEE J. Sel. Top. Quantum Electron.* **2018**, *24*, 8300707. [[CrossRef](#)]
140. He, J.; Dong, T.; Xu, Y. Review of Photonic Integrated Optical Phased Arrays for Space Optical Communication. *IEEE Access* **2020**, *8*, 188284–188298. [[CrossRef](#)]
141. Brassard, G.; Bennett, C.H. Quantum cryptography: Public key distribution and coin tossing. In Proceedings of the IEEE international conference on computers, systems, and signal processing, Bangalore, India, 9–12 December 1984; pp. 175–179.
142. Bennett, C.H. Quantum cryptography: Uncertainty in the service of privacy. *Science* **1992**, *257*, 752–753. [[CrossRef](#)]
143. Ekert, A.K. Quantum cryptography based on Bell's theorem. *Phys. Rev. Lett.* **1991**, *67*, 661–663. [[CrossRef](#)]
144. Djordjevic, I.B. *Physical-Layer Security and Quantum Key Distribution*; Springer: Berlin/Heidelberg, Germany, 2019.
145. Chou, H.H.; Huang, W.T. Wavelength Tunable Asymmetric B-OWC System Based on Self-Injection Locking for TDM-PONs. *IEEE Photonics Technol. Lett.* **2021**, *33*, 370–372. [[CrossRef](#)]
146. Xia, X.-X.; Zhang, Z.; Xie, H.-B.; Yuan, X.; Lin, J.; Liao, S.-K.; Liu, Y.; Peng, C.-Z.; Zhang, Q.; Pan, J.-W. LED-based fiber quantum key distribution: Toward low-cost applications. *Photon. Res.* **2019**, *7*, 1169–1174. [[CrossRef](#)]
147. Lo, H.-K.; Ma, X.; Chen, K. Decoy State Quantum Key Distribution. *Phys. Rev. Lett.* **2005**, *94*, 230504. [[CrossRef](#)] [[PubMed](#)]
148. Wootters, W.K.; Zurek, W.H. A single quantum cannot be cloned. *Nature* **1982**, *299*, 802–803. [[CrossRef](#)]